Article

Neuron

Menin Deficiency Leads to Depressive-like Behaviors in Mice by Modulating Astrocyte-Mediated Neuroinflammation

Highlights

- Astroglia menin deficiency leads to depressive-like behaviors in mice
- Menin reduction in astrocytes promotes IL-1β generation through NF-κB activation
- NF-κB and IL-1β inhibitors attenuate the depressive-like phenotypes
- A *MEN1* SNP associated with MDD risk leads to aberrant NF-κB activation

Authors

Lige Leng, Kai Zhuang, Zeyue Liu, ..., Huaxi Xu, Qi Xu, Jie Zhang

Correspondence

xuqi@pumc.edu.cn (Q.X.), jiezhang@xmu.edu.cn (J.Z.)

In Brief

Mechanisms underlying astrocyte-mediated neuroinflammation in depression remain unclear. Menin regulates NF-κB activity in astrocytes to promote neuroinflammation. Clinically, a *MEN1* SNP is associated with the onset of depression. This study reveals a distinct role for menin in neuroinflammation and depression.

Leng et al., 2018, Neuron *100*, 1–13
November 7, 2018
https://doi.org/10.1016/j.neuron.2018.08.031

CellPress

Please cite this article in press as: Leng et al., Menin Deficiency Leads to Depressive-like Behaviors in Mice by Modulating Astrocyte-Mediated Neuroinflammation, Neuron (2018), https://doi.org/10.1016/j.neuron.2018.08.031

Neuron
Article

Menin Deficiency Leads to Depressive-like Behaviors in Mice by Modulating Astrocyte-Mediated Neuroinflammation

Lige Leng,[1,9] Kai Zhuang,[1,9] Zeyue Liu,[2,9] Changquan Huang,[1] Yuehong Gao,[1] Guimiao Chen,[1] Hui Lin,[1] Yu Hu,[1] Di Wu,[1] Meng Shi,[1] Wenting Xie,[1] Hao Sun,[1] Zhicheng Shao,[1] Huifang Li,[1] Kunkun Zhang,[3] Wei Mo,[3] Timothy Y. Huang,[4] Maoqiang Xue,[5] Zengqiang Yuan,[6] Xia Zhang,[7] Guojun Bu,[1,8] Huaxi Xu,[1,4] Qi Xu,[2,*] and Jie Zhang[1,10,*]

[1]Fujian Provincial Key Laboratory of Neurodegenerative Disease and Aging Research, Institute of Neuroscience, College of Medicine, Xiamen University, Xiamen, Fujian 361102, P.R. China
[2]State Key Laboratory of Medical Molecular Biology, Institute of Basic Medical Sciences Chinese Academy of Medical Sciences and Peking Union Medical College, Neuroscience Center, Chinese Academy of Medical Sciences, Beijing 100005, P.R. China
[3]School of Life Sciences, Xiamen University, Xiamen, Fujian 361102, P.R. China
[4]Neuroscience Initiative, Sanford Burnham Prebys Medical Discovery Institute, La Jolla, CA 92037, USA
[5]Department of Basic Medical Science, Medical College, Xiamen University, Xiamen, Fujian 361102, P.R. China
[6]The Brain Science Center, Beijing Institute of Basic Medical Sciences, Beijing 100850, P.R. China
[7]Institute of Mental Health Research at the Royal and Departments of Psychiatry and Cellular and Molecular Medicine, University of Ottawa, Ottawa, ON K1Z7K4, Canada
[8]Department of Neuroscience, Mayo Clinic, Jacksonville, FL 32224, USA
[9]These authors contributed equally
[10]Lead Contact
*Correspondence: xuqi@pumc.edu.cn (Q.X.), jiezhang@xmu.edu.cn (J.Z.)
https://doi.org/10.1016/j.neuron.2018.08.031

SUMMARY

Astrocyte dysfunction and inflammation are associated with the pathogenesis of major depressive disorder (MDD). However, the mechanisms underlying these effects remain largely unknown. Here, we found that multiple endocrine neoplasia type 1 (*Men1*; protein: menin) expression is attenuated in the brain of mice exposed to CUMS (chronic unpredictable mild stress) or lipopolysaccharide. Astrocyte-specific reduction of *Men1* (GcKO) led to depressive-like behaviors in mice. We observed enhanced NF-κB activation and IL-1β production with menin deficiency in astrocytes, where depressive-like behaviors in GcKO mice were restored by NF-κB inhibitor or IL-1β receptor antagonist. Importantly, we identified a SNP, rs375804228, in human *MEN1*, where G503D substitution is associated with a higher risk of MDD onset. G503D substitution abolished menin-p65 interactions, thereby enhancing NF-κB activation and IL-1β production. Our results reveal a distinct astroglial role for menin in regulating neuroinflammation in depression, indicating that menin may be an attractive therapeutic target in MDD.

INTRODUCTION

Major depressive disorder (MDD) affects approximately 16% of the population and has become the main cause of disability worldwide (CONVERGE consortium, 2015; Ferrari et al., 2013). Despite the high prevalence of this disorder, mechanisms underlying MDD risk remain elusive. MDD is characterized by mood despondency, disinterest, loss of concentration, and increased propensity for suicidal thoughts (Canals et al., 2002). MDD was initially speculated to be a neuropsychiatric disease derived from neuronal dysfunction (Manji et al., 2001). However, numerous studies have now implicated astrocyte dysfunction in the pathogenesis of MDD (Rajkowska and Stockmeier, 2013; Sanacora and Banasr, 2013; Wang et al., 2017). As the most abundant glial cell type in the mammalian brain, astrocytes produce pro-inflammatory cytokines such as interleukin (IL)-1β, which are key to the induction of depressive symptoms in MDD (Koo and Duman, 2009; Norman et al., 2010). As a pro-inflammatory transcriptional activator, nuclear factor-κB (NF-κB) is a critical regulator of inflammation in the central nervous system (CNS) (Baltimore, 2011; Oeckinghaus and Ghosh, 2009); however, the pathogenic driver of NF-κB-dependent pro-inflammatory activation in astrocytes during MDD onset remains unclear.

Recent studies suggest that dysregulation of genes residing within the chromosome 11q13.1 locus can mediate abnormal NF-κB activation (Parker et al., 2014). In support of this, chromosomal micro-deletion of 11q13.1 was detected in a patient diagnosed with mental retardation (Gimelli et al., 2011). Among the 12 genes deleted in 11q13.1, the multiple endocrine neoplasia type 1 gene (*MEN1*; encoding the protein menin) was of particular interest. Loss-of-function *MEN1* gene mutations are causal to MEN1 syndrome, which is a dominantly inherited disease characterized by tumor formation in endocrine organs (Matkar et al., 2013). MEN1 patients also feature neurological irregularities such as depression (Aoki et al., 1997). As a scaffold component of nuclear protein complexes, menin has been shown to

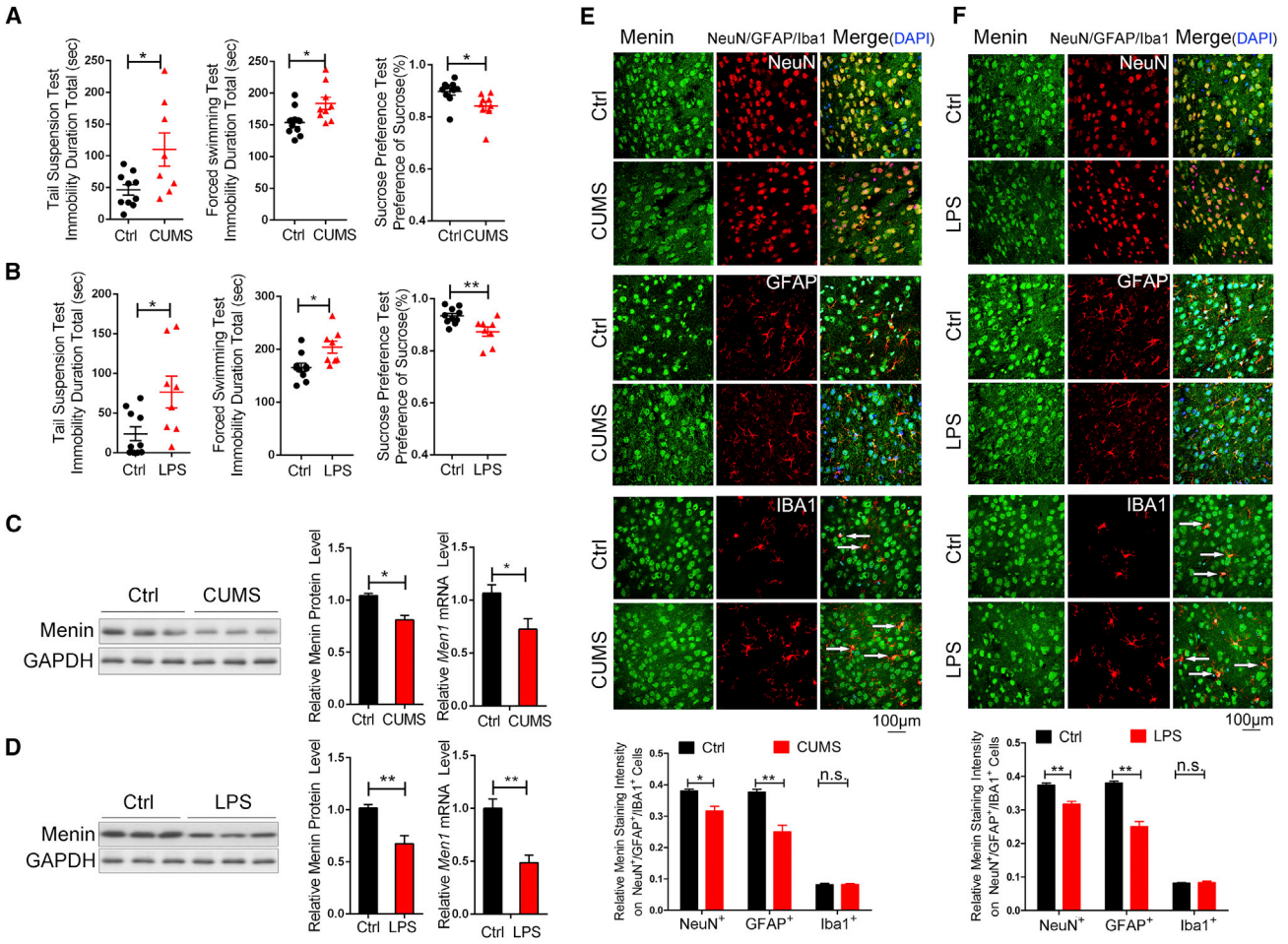

Figure 1. Menin Levels Are Attenuated in Mouse Brain after CUMS and LPS Induction

Male C57BL/6 mice were exposed to chronic unpredictable mild stress (CUMS) or LPS induction.

(A and B) CUMS- (A) and LPS- (B) treated mice and Ctrl mice behaviors in TSTs, FSTs, and SPTs (CUMS, n = 10 mice; Ctrl, n = 8 mice; LPS treated, n = 9 mice; Ctrl, n = 9 mice).

(C and D) *Men1* mRNA and protein levels in CUMS/control (C) and LPS-treated/control (D) mouse brains. n = 3 experimental replicates/group.

(E and F) Cortical sections of CUMS/control (E) or LPS-treated/control (F) mouse brain, stained to visualize menin (green) with NeuN (red), GFAP (red), or IBA1 (red) as indicated to characterize menin expression in neurons, astrocytes, or microglia (scale bar, 100 μm). Staining intensity is quantified as shown in the lower panels.

Data represent mean ± SEM; n.s., not significant; *p < 0.05, **p < 0.01, ***p < 0.001, one-way ANOVA with Turkey's post hoc test.

See also Figures S1 and S2.

modulate gene expression and cell signaling during tumorigenesis (Heppner et al., 2001; Matkar et al., 2013), potentially through interactions with the p65 NF-κB subunit (Gang et al., 2013; Heppner et al., 2001). Although menin is ubiquitously expressed, its function differs according to tissue and cell type (Fang et al., 2013; Matkar et al., 2013). However, a function for menin in the CNS has been largely unexplored.

Here, we provide strong evidence that menin deficiency increases NF-κB-induced IL-1β levels in astroglia to promote inflammation and associated onset of depressive-like phenotypes. A SNP associated with *MEN1* (rs375804228) is linked to NF-κB hyper-activation and MDD susceptibility. Together, our results reveal a distinct role for the tumor suppressor menin in regulating astroglial inflammation in depressive disorders.

RESULTS

Menin Levels Are Attenuated in Mouse Brain after CUMS and LPS Exposure

Chronic stress and neuroinflammation are thought to be fundamental in the etiology of MDD. To explore intermediary components that are modulated by stress and neuroinflammation, we exposed male C57BL/6 mice to 6 weeks of chronic unpredictable mild stress (CUMS) or 10 days of lipopolysaccharide (LPS) intraperitoneal injection to mimic depression. Depressive-like phenotypes in these models were validated by tail suspension tests (TSTs) (Can et al., 2012), forced swimming tests (FSTs) (Chatterjee et al., 2012), and sucrose preference tests (SPTs) (Figures 1A and 1B). We found that *Men1* protein and

mRNA levels are significantly attenuated in cortex from both CUMS- and LPS-treated mice by western blotting and RT-PCR (Figures 1C and 1D). Immunostaining also revealed that menin is markedly decreased in neurons and astrocytes (arrows) in mouse brain after CUMS and LPS treatment. Menin expression was relatively low in microglia (arrows) and little difference in microglia abundance was observed with CUMS or LPS treatment (Figures 1E and 1F). The nucleus accumbens (NAc) is an important brain region in depression, where menin levels are also significantly decreased in NAc of CUMS mouse brain (Figure S1A). These results suggest that menin may be involved in chronic stress, neuroinflammation, and consequent depressive-like phenotypes.

Generation of *Men1* Brain Cell-Type-Specific Conditional Knockout Mice

Men1 expression can be detected in most mouse organs from gestational day 7, including the brain (Matkar et al., 2013). Comparing menin expression in cultured neurons, microglia, astrocytes, and oligodendrocytes (Figure S2A), we found that menin expression was relatively high in neurons and astrocytes. Interestingly, menin expression was most predominant in astrocytes (Figures S2B and S2C). By immunostaining, we confirmed that very little menin can be detected in microglia and oligodendrocytes in mouse cortex (Figures 1E, 1F, and S2D). MBP (myelin basic protein) staining also reveals no difference in myelination between astrocyte plus neural progenitor cell-specific (GcKO) and control (Ctrl) mouse cortex and hippocampus (Figure S2E). To investigate potential astrocyte- or neuron-specific effects associated with depressive-like phenotypes derived from *Men1* gene deletion, we generated CNS-specific whole-brain (NcKO), neuron-specific (CcKO), and GcKO *Men1* deletion mouse lines by crossing the floxed *Men1* allele with *Nestin-Cre*, *CamkII*α*-cre*, or *GFAP-Cre* transgenic lines (Akbarian et al., 2002; Scacheri et al., 2004; Tronche et al., 1999; Trumpp et al., 1999; Westerman et al., 2012), respectively (Figure 2A). Global *Men1* deletion in the CNS resulted in early postnatal lethality (Zhuang et al., 2018); therefore, we used heterozygous *Men1* deletion strains generated by *Nestin-Cre* crosses (*Nestin-Cre*, $Men1^{f/+}$) for comparison. *Men1* CcKO and GcKO animals exhibited normal growth rate; body and brain sizes, in addition to longevity, were indistinguishable from Ctrls ($Men1^{f/f}$ animals were used as Ctrls) (Figures S3A–S3C) (Zhuang et al., 2018). To confirm astrocyte-specific menin reduction in GcKO transgenic animals, we performed menin/glial fibrillary acidic protein (GFAP) and menin/NeuN double staining in GcKO brain cortex. GFAP-labeled astrocytes featured attenuated menin staining, while neuronal menin expression was minimally affected in GcKO mice compared to Ctrls (Figures S3D–S3F). No appreciable differences in cortical structure were observed between GcKO and Ctrl mice by Nissl staining (Figure S3G). Altogether, these findings suggest that postnatal deletion of menin in brain has minimal effects on overall brain development in mice.

Mice with Astroglial *Men1* Reduction Exhibit Depressive-like Behaviors

We then assessed potential depressive-like behaviors in *Men1* NcKO, CcKO, and GcKO mice using TSTs (Can et al., 2012), FSTs (Chatterjee et al., 2012), SPTs, and sucrose consumption tests (SCTs) (Gross and Pinhasov, 2016). Surprisingly, NcKO and GcKO mice showed a significant increase in immobility duration during TSTs and FSTs, whereas CcKO animals showed little or no variation compared to Ctrls (Figures 2B and 2C). Furthermore, NcKO and GcKO animals exhibited less preference to sucrose in SPT and SCT trials, with no effect observed in CcKO animals (Figures 2D–2F). These results indicate that mice with menin reduction in astrocytes (NcKO and GcKO lines), but not in neurons (CcKO), manifest depressive-like phenotypes. Impaired social interactivity is also characteristically seen in MDD; social interactions in GcKO mice were also found to be impaired in the presence of novel interaction partners during social interaction tests (SITs) (Figures 2G and 2H).

GcKO animals exhibited reduced general locomotion in open field tests and plus maze assays, with no differences observed in motor coordination in rotarod tests, and anxiety-like behavior in open field and elevated plus maze assays (Figures S4A–S4C). Since reduced locomotor activity may be due to depressive or motivational deficits in GcKO animals, we performed Morris water maze tests to further characterize cognitive behavior. GcKO mice did not exhibit significant differences in learning and memory, or swimming speed and distance compared to Ctrl mice (Figures S4D and S4E), indicating that astroglial reduction of menin had no effect on forced locomotor activity, anxiety, or learning and memory.

To further determine whether astrocytic menin is critical for depressive-like behaviors, we used an *Fgfr3-iCre(ER)* mouse line in which CreER is expressed from an *Fgfr3* promoter and activation of the Cre recombinase is induced by tamoxifin, resulting in menin reduction in forebrain subventricular zone progenitor cells and astrocytes (Rivers et al., 2008). Tamoxifin-induced astrocyte-specific *Men1* KO mouse lines were generated by crossing $Men1^{f/f}$ and *Fgfr3-iCre(ER)* mouse lines, hereby referred to as FcKO (Figure 2A). Astroglial menin levels were substantially decreased in FcKO mice compared to Ctrls with tamoxifin treatment (Figures S3H and S3I), with no significant effects observed on brain weight (Figure S3J). As expected, FcKO mice also exhibited depressive-like phenotypes as determined by TST and FST trials (Figure 2I). Together, these results suggest that menin deficiency in astrocytes promotes depressive-like phenotypes in mice.

Astrocytic Menin Reduction Promotes IL-1β Production through NF-κB Activation

To explore molecular mechanisms associated with the phenotypes observed upon astrocyte *Men1* reduction, we examined mRNA expression profiles by RNA sequencing (RNA-seq) analysis in primary cultured astrocytes derived from Ctrl and GcKO mice using a BGISEQ-500 platform. Altogether, 562 genes showed altered expression in 3/3 samples (>2-fold difference to Ctrls, FDR-corrected $p < 0.001$; Figure 3A). GO biological process analysis indicates that cytokine-cytokine receptor interaction was significantly represented within the dataset (Figure 3B, RED). This implicates potential modulation of the neuroinflammatory response with astroglial menin reduction.

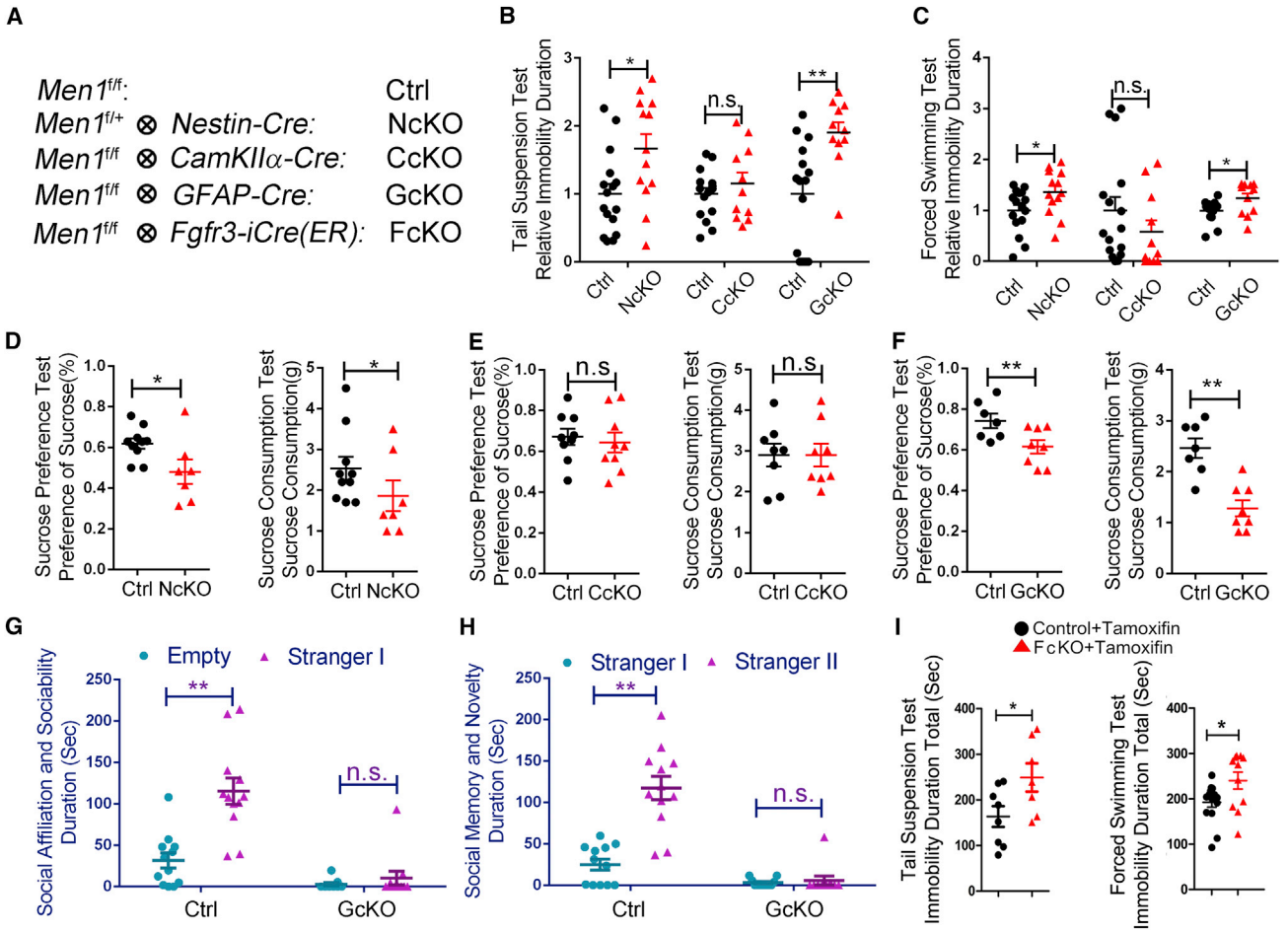

Figure 2. Astroglial *Men1* Reduction Results in Depressive-like Behavior in Mice

(A) Generation of conditional *Men1* knockout mice by crossing *Men1*$^{f/f}$ lines with *Nestin-cre*, *CamKIIα-cre*, *GFAP-cre*, or *Fgfr3-iCre(ER)* mouse lines. Resulting *Men1* cKO mouse lines are referred to as NcKO, CcKO, GcKO, or FcKO lines, respectively.

(B and C) Behavioral analysis of NcKO, CcKO, GcKO, and littermate Ctrls using TSTs (B) and FSTs (C).

(D–F) Behavioral analysis of NcKO (D), CcKO (E), GcKO (F), and littermate Ctrls using SPTs and SCTs.

(G and H) Behavioral analysis of GcKO and littermate Ctrls using SITs.

(G) Social affiliation and sociability. Mean duration in the chamber with a novel mouse ("Stranger I"-containing chamber) compared to the opposite chamber ("Empty" chamber).

(H) Social memory and novelty. Mean duration spent in the chamber with the mouse from the sociability phase ("Stranger I"), and in the opposite chamber with a new unfamiliar mouse ("Stranger II").

(I) FcKO and littermate Ctrl behaviors in TSTs and FSTs.

Number of mice used in behavior tests: NcKO group, Ctrl, n = 17 mice; NcKO, n = 13 mice; CcKO group, Ctrl, n = 16 mice; CcKO, n = 13 mice; GcKO group, Ctrl, n = 15 mice; GcKO, n = 12 mice; FcKO group, Ctrl, n = 10 mice; FcKO, n = 10 mice. Data represent mean ± SEM; n.s., not significant; *p < 0.05, **p < 0.01, ***p < 0.001, one-way ANOVA with Tukey's post hoc analysis.

See also Figures S2–S4.

Neuroinflammation is tightly associated with the onset of depression (Fenn et al., 2014; Skaper et al., 2014). Given that astrocytic menin reduction results in depressive-like behaviors, it seems likely that astroglial neuroinflammatory mechanisms may drive depressive-like phenotypes in GcKO mice. As predicted, many pro-inflammatory factors including IL-1β were significantly upregulated in astrocytes derived from cortex of GcKO compared to Ctrl mice (Figure 3C). Given that IL-1β is a key pro-inflammatory cytokine involved in the induction of depressive-like behaviors (Koo and Duman, 2009; Norman et al., 2010), we confirmed that IL-1β mRNA levels were indeed dramatically enhanced in cortex of GcKO and NcKO mice, but not in CcKO mice (Figure 3D). IL-1β mRNA levels were also enhanced in the NAc of CUMS mouse brain (Figure S1B). Next, we measured IL-1β levels in cultured primary astrocytes and neurons derived from cortex in *Men1*-NcKO mice and littermate Ctrls. In agreement with our results *in vivo*, we detected higher basal IL-1β mRNA levels in Ctrl astroglial cultures compared to Ctrl neuronal cultures (Figure 3E). Neuronal menin reduction did not affect IL-1β expression in neuronal cultures;

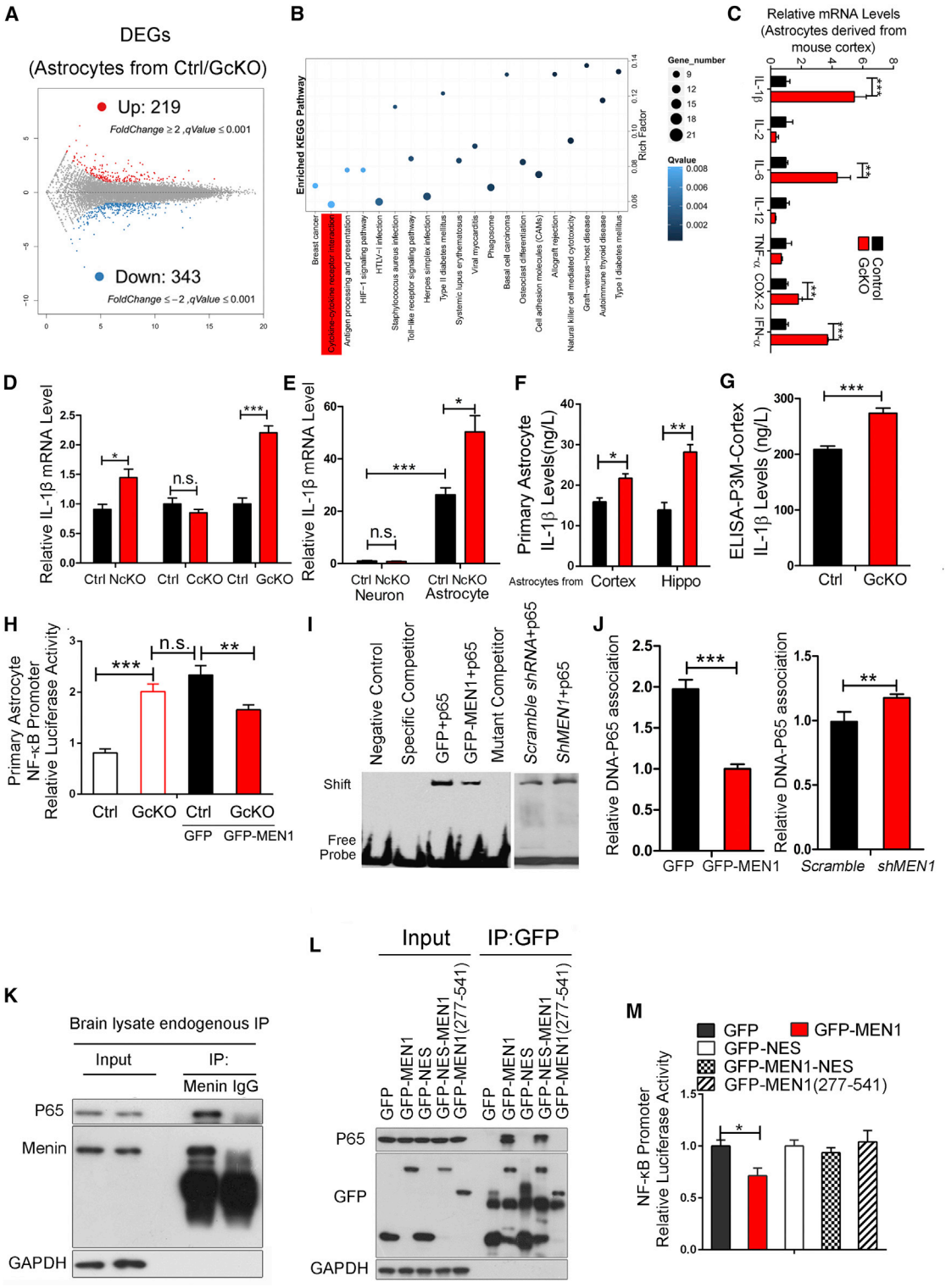

Figure 3. Loss of Menin Enhances IL-1β Production through NF-κB Induction

(A) Differentially expressed genes (DEGs) identified from astrocytes derived from cortex of Ctrl and GcKO mice. Red plots represent upregulated DEGs. Blue plots represent downregulated DEGs. Gray points represent non-DEGs. The detailed RNA-seq data have been deposited in the SRA database and can be found at SRA: SRP151969.

(B) Enriched KEGG pathway in DEGs. The cytokine/cytokine receptor interaction pathway is significantly enriched (red rectangle).

(legend continued on next page)

however, menin reduction in astrocytes resulted in an ~2-fold increase in IL-1β expression (NcKO astrocytes compared to Ctrls; Figure 3E). Elevations in astroglial IL-1β and reduced menin levels were further confirmed by measuring IL-1β levels in conditioned media from Ctrl and *Men1* KO cortical or hippocampal astroglial cultures (Figure 3F), as well as cortical brain lysates from GcKO and Ctrl mice (Figure 3G). Microglia cells are sensitive to neuroinflammation and are fundamentally involved in the production of pro-inflammatory cytokines (Brambilla et al., 2005; Farina et al., 2007). We observed enhanced activation of microglia in cortex of GcKO mice, with little or no change in proliferation (Figures S5A and S5B). Thus, microglial activation by astrocyte-derived pro-inflammatory cytokines likely exacerbates neuroinflammation in GcKO mice.

The IL-1β promoter region comprises classical NF-κB binding sites and has been well characterized as a downstream NF-κB target (Cogswell et al., 1994). Since astrocytes have been shown to mediate inflammation through the NF-κB pathway (Herkenham et al., 2011; Mao et al., 2009), we determined whether menin reduction can activate NF-κB in astrocytes. To test this, we measured NF-κB luciferase reporter activity in *Men1*-deficient astrocytes and observed a significant increase in NF-κB-mediated transactivation (Figure 3H). Conversely, menin overexpression in *Men1*-deficient astrocytes suppressed NF-κB-mediated transactivation (Figure 3H). Using an astrocytic cell line stably expressing menin (CHG-5-MEN1), we observed a decrease in IL-1β mRNA and protein levels, with attenuated NF-κB-mediated transactivation in CHG-5-MEN1 cells compared to CHG-5-vector Ctrls (Figures S6A–S6C). Similar results were observed in HEK293T cells: while menin overexpression inhibited NF-κB-mediated transactivation, *MEN1* knockdown enhanced NFκB-mediated transactivation (Figures S6D–S6F). Additionally, menin overexpression inhibited NF-κB-mediated transactivation induced by LPS exposure (Figure S6G), further indicating that menin can suppress NF-κB-dependent transactivation.

Nuclear p65 translocation can directly enhance NFκB-mediated transactivation. To determine whether menin reduction affects nuclear p65 translocation, we examined changes in p65 distribution by comparing enriched nuclear and cytoplasmic fractions. No obvious difference in nuclear p65 distribution was observed in brain cortex comparing GcKO and Ctrl groups (Figure S6H). Similarly, menin overexpression in CHG-5 cells also had no effect on nuclear p65 distribution (Figure S6I). These results suggest that menin deficiency does not affect p65 nuclear translocation.

Next, we determined whether menin directly affects p65/DNA binding. Significantly, menin overexpression decreased p65 binding activity as determined by electrophoretic mobility shift assay (EMSA), while *Men1* knockdown conversely enhanced p65/DNA binding interactions (Figures 3I and 3J). Further, menin and p65 was co-immunoprecipitated from mouse brain tissue lysates (Figure 3K), indicating that menin and p65 could interact within a protein complex. Cytoplasmic menin showed no effect in inhibiting NF-κB-mediated transactivation; although cytoplasmic menin constructs (menin fused to a nuclear export signal, NES) showed interactions with p65, no effects on NF-κB were observed with these constructs (Figure 3L). In mapping the regions required for menin/p65 interaction, a 277–541 amino acid region in menin was found to be crucial for p65 binding; menin constructs lacking this region abolished menin-mediated inhibition on NF-κB-dependent transactivation (Figure 3M). These results suggest that menin suppresses NF-κB activation through its association with p65, thereby inhibiting p65-DNA binding.

NF-κB Inhibitor and IL-1β Receptor Antagonist Ameliorate Depressive-like Behaviors in GcKO Mice

To determine whether inhibiting the NF-κB/IL-1β pathway can rescue depressive-like behaviors in GcKO mice, we treated GcKO and Ctrl mice with an NF-κB inhibitor, pyrrolidine dithiocarbamate (PDTC), or an IL-1β receptor antagonist (IL-1β-RA) by intraperitoneal injection for 7 days (Figure 4A). We found that both PDTC and IL-1β-RA treatment significantly decreased immobility in GcKO mice in TST and FST trials (Figures 4B–4E), and rescued SPT and SCT behaviors (Figures 4F and 4G) in GcKO mice. Further, social interaction deficits were completely rescued by PDTC administration (Figures 4H and 4I). IL-1β-RA significantly enhanced primary contact with novel mice, with no effects on a second novel mouse (Figures 4J and 4K). Ctrl mice treated with PDTC or IL-1β-RA did not exhibit any significant behavioral differences in TST, FST, SIT, SPT, and SCT trials (Figure 4). These results indicate that PDTC and IL-1β-RA significantly rescued depressive-like behavioral deficits in GcKO mice, with little adverse side effects observed in Ctrls.

(C) Expression of inflammatory cytokines in astrocytes derived from cortex of GcKO and Ctrl mice.
(D) qRT-PCR measurements to determine IL-1β expression levels in hippocampal samples from 2-month-old NcKO, CcKO, and GcKO mice and their littermate Ctrls. n = 6 experimental replicates/group.
(E) IL-1β mRNA levels in primary cortical neurons and astrocytes from Ctrl and NcKO mice. n = 4 experimental replicates/group.
(F and G) IL-1β protein levels in astrocytes derived from cortex and hippocampus (F) or in brain cortex lysates (G) as determined by ELISA. n = 4 experimental replicates/group.
(H) Astrocytes derived from GcKO or Ctrl mice transfected with GFP or GFP-MEN1; NFκB-mediated transactivation was measured by luciferase assay.
(I and J) p65 DNA binding capacity was measured by EMSA in HEK293T cells after transfection with the plasmids indicated. Quantification of panels in (I) are shown in (J); n = 3 experimental replicates/group.
(K) Menin/p65 interactions were measured in mouse brain by endogenous co-immunoprecipitation (coIP).
(L) HEK293T cells were co-transfected with p65 together with GFP, GFP-MEN1, GFP-NES, GFP-NES-MEN1, or GFP-MEN1 (277-541) constructs. Interactions between p65 with menin were determined by coIP; antibodies used in the IP reactions are indicated.
(M) NFκB-mediated transactivation in astrocytes transfected with plasmid constructs as indicated.
Data represent mean ± SEM; n.s., not significant; *p < 0.05, **p < 0.01, ***p < 0.001, one-way ANOVA with Tukey's post hoc analysis.
See also Figure S1, S5, and S6.

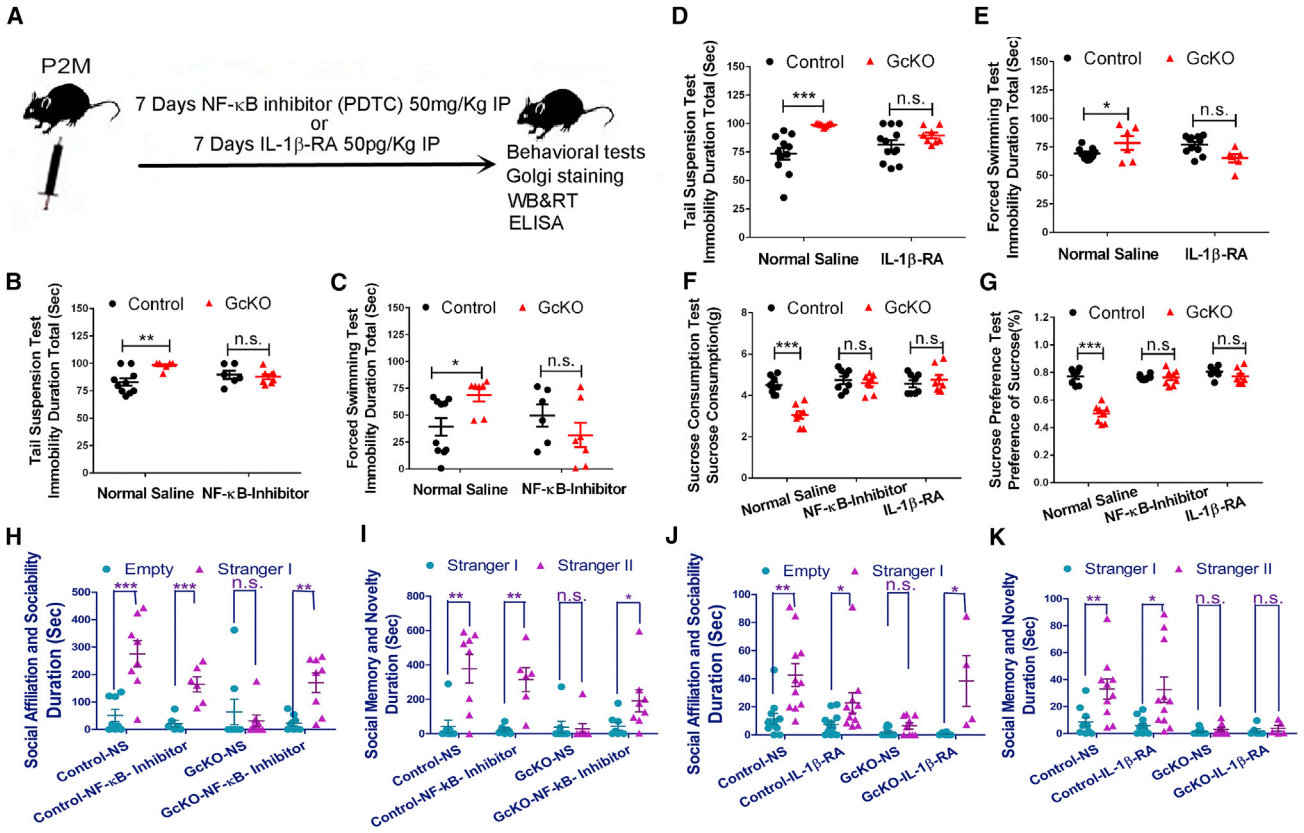

Figure 4. NF-κB Inhibitor and IL-1β Receptor Antagonist Ameliorate Depressive-like Behavior in GcKO Mice

(A) Two-month-old GcKO and littermate Ctrl mice treated with an NF-κB inhibitor (PDTC) or an IL-1β receptor antagonist (IL-1β-RA) for 7 days, whereby mice were subjected to behavioral analysis and following experiments as indicated.

(B–G) Behavioral analysis of PDTC-, IL-1β-RA-, or saline-treated GcKO and littermate Ctrls by TSTs (B and D), FSTs (C and E), SCTs (F), and SPTs (G). Number of mice used in behavior tests: (B) and (C), control+normal saline group, n = 10 mice; control+NF-κB inhibitor group, n = 6 mice; GcKO+normal saline group, n = 7 mice; GcKO+NF-κB inhibitor group, n = 7 mice; (D) and (E), control+normal saline group, n = 11 mice; control+IL-1β-R-A group, n = 13 mice; GcKO+normal saline group, n = 6 mice; GcKO+IL-1β-RA group, n = 7 mice; (F) and (G), n = 8 mice for each group.

(H–K) PDTC/saline- (H and I) or IL-1β-RA/saline- (J and K) treated GcKO and littermate Ctrls in social affiliation and sociability assays.

Data represent mean ± SEM; n.s., not significant; *p < 0.05, **p < 0.01, ***p < 0.001, one-way ANOVA with Tukey's post hoc analysis.

IL-1β-RA Rescues Neuronal Morphological Abnormalities and Synaptic Deficits Induced by Astroglial Menin Reduction

Astrocytes provide neurons with morphogenic and metabolic support and are fundamental to the functional regulation of dendritic spines (Allen, 2014). Using a co-culture system comprising primary Ctrl or *Men1* KO astrocytes cultured with Ctrl primary neurons, we assayed effects of astrocytic menin reduction on neuronal dendritic morphology, as indicated by microtubule-associated protein 2 (MAP2) staining (Figure 5A). Interestingly, dendritic complexity and total length (Figures 5A and 5B) were reduced in neurons cultured with *Men1* KO astrocytes. Ionotropic glutamate receptor subunits (GluR1 and NR2A) and synaptic components (postsynaptic density protein 95 [PSD95]) were also dramatically decreased in neurons co-cultured with *Men1* KO astrocytes (Figures 5C and 5D). Importantly, treatment of *Men1* KO astrocyte/neuron co-cultures with IL-1β-RA restored neuronal dendritic complexity, total dendritic length, and synaptic protein expression (Figures 5A–5D). Further, Golgi staining in GcKO mouse cortex and hippocampus revealed significant attenuation in dendritic branching, while IL-1β-RA treatment significantly improved dendritic complexity (Figures 5E and 5F). Expression of GluR1, NR2A, PSD95, and IL-1β levels was also restored in cortex and hippocampus of GcKO mouse brain (Figure S7). Furthermore, microglia activation was attenuated (Figures S5C and S5D), indicating that attenuation of neuroinflammatory response in GcKO brain is ameliorated with IL-1β-RA treatment. Further, serotonin levels were markedly decreased in cortex of GcKO mice, while IL-1β-RA normalized serotonin levels (Figure 5G).

Dendritic arbor and complexity tightly correlate with neuronal function, and deficits in hippocampal neural plasticity are also associated with mouse models of depression (Castrén, 2013; Christoffel et al., 2011). We compared hippocampal-dependent long-term potentiation (LTP) in acute brain slices derived from GcKO and Ctrl mice. Notably, LTP was dramatically impaired in GcKO mice compared with Ctrls. Moreover, LTP deficiencies were rescued by exposure to IL-1β-RA in cultured hippocampal slices by electrophysiological analysis (Figures 5H and 5I).

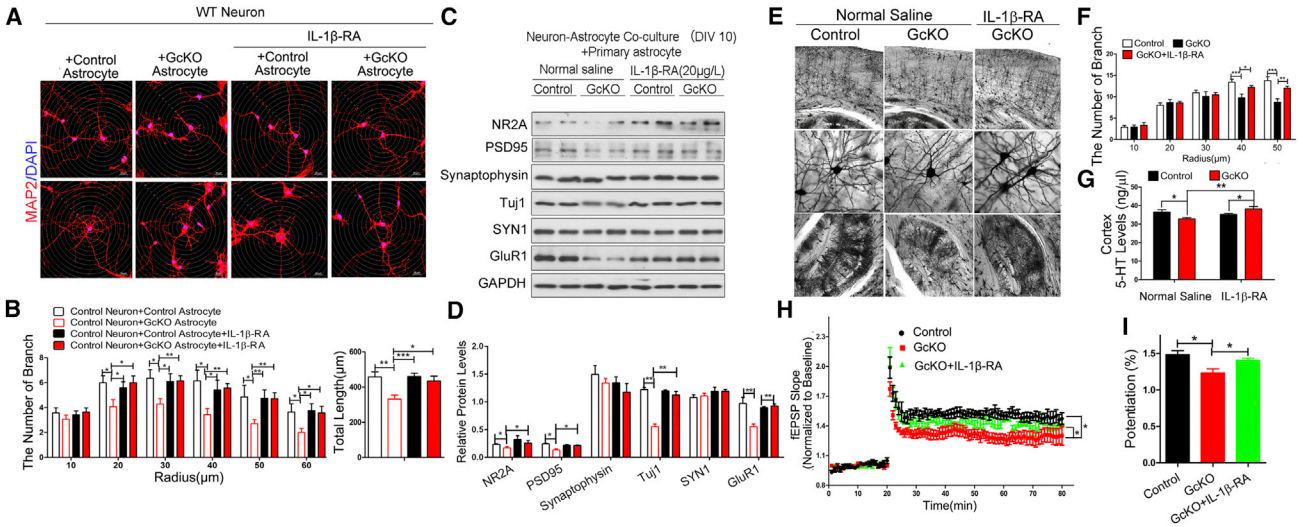

Figure 5. IL-1β Receptor Antagonist Rescues Morphological Abnormalities and Synaptic Deficits in Neurons Induced by Astrocytic Menin Reduction

(A and B) WT neurons co-cultured with Ctrl or *Men1* KO astrocytes treated with or without IL-1β-RA; neurons were immunostained with an anti-MAP2 antibody. Representative confocal projection images of dendritic complexity are shown in (A). Scale bar, 20 μm. (B) Quantitation of total dendritic length and dendritic complexity. n = 20 neurons.

(C and D) Western blot analysis of protein expression in neurons co-cultured with WT or *Men1* KO astrocytes treated with or without IL-1β-RA. Immunoblots were probed with antibodies against the indicated proteins. Quantification of proteins levels is shown in (D); n = 4 experimental replicates/group.

(E and F) Two-month-old GcKO mice treated with IL-1β-RA for 7 days; untreated and IL-1β-RA-treated GcKO and littermate Ctrl lines were subjected to Golgi staining (three mice were used for every group). Representative Golgi staining from cortex and hippocampal CA1 regions is shown. Scale bar, 10, 100, and 20 μm, respectively. (F) Quantitation of dendritic complexity in neurons from above mice. n = 20 neurons.

(G) Hippocampal serotonin (5-HT) levels from GcKO or Ctrl mice treated with saline or IL-1β-RA as determined by ELISA. n = 5 experimental replicates/group.

(B–G) Data represent mean ± SEM, *p < 0.05, **p < 0.01, ***p < 0.001, one-way ANOVA with Tukey's post hoc analysis.

(H and I) LTP recordings from Ctrl and GcKO mouse brain (n = 8 slices from 4 Ctrl mice; 9 slices from 5 CcKO mice; 8 slices from 5 CcKO mice treated with IL-1β-RA.).

(H) LTP was induced by two trains of 100-Hz stimuli in the Schaffer collaterals.

(I) Significant differences in fEPSP potentiation were determined by comparing fEPSP slopes during last 10 min of recording after high-frequency stimulation. Data represent mean ± SEM, *p < 0.05, one-way ANOVA with Holm-Sidak pairwise tests.

See also Figures S5 and S7.

A *MEN1* SNP Is Associated with MDD Risk

Loss-of-function *MEN1* gene mutations are commonly observed in MEN1 syndrome patients (Chandrasekharappa et al., 1997). To determine whether *MEN1* mutations are associated with the development of MDD in humans, we genotyped the *MEN1* coding region on chromosome 11q13.1 in a total of 1,032 patients with MDD and 866 Ctrls. Subjects with MDD and corresponding Ctrls were age- and sex-matched (Table 1). Within the analyzed cohort, approximately 18% of the MDD patients reported MDD in multiple members within their family lineage. In nine SNPs identified within the *MEN1* coding region (Table 2), only one of these SNPs (T-allele of rs375804228) was associated with MDD susceptibility by chi-square test (χ^2 = 7.236, p = 0.00715, odds ratio [OR] = 3.208, 95% confidence interval [95% CI], 1.37–7.50). The rs375804228 polymorphism resides on exon 10 in the *Men1* locus, and the T-variant of this allele results in a G503D substitution (Table 2). Two other SNPs, rs2071313 and rs2959656, are common polymorphisms, with a prevalence of approximately 20% and 42%, respectively (Concolino et al., 2016; Lemos and Thakker, 2008) (Table 2). The rs2071313 polymorphism resides on exon 9 and is a non-coding variant (D418D) (Bazzi et al., 2008), while rs2959656 (A/G) results in a benign amino acid substitution (A541T) (Bazzi et al., 2008).

Table 1. Clinical Information of Subjects Used in This Study

	Case	Control
Number of subjects	1,032	866
Sex (male/female)	439/593	381/485
Age (years)	37 ± 13.59	40.86 ± 14.06
Age of onset (years)	34 ± 13.45	N/A
First-episode patients	206 (19.96%)	N/A
Family history of MDD	183 (17.73%)	N/A

To investigate the possibility that rs375804228 (G503D) is involved in MDD, we generated menin GFP-tagged wild-type (WT) and G503D (GFP-MEN1-G503D) expression vectors. GFP-MEN1-D418D and GFP-MEN1-A541T constructs were used as Ctrls. We observed no significant difference in *MEN1* mRNA or protein expression levels in WT- and G503D-menin constructs (Figures S8A and S8B). Moreover, we observed no difference in protein stability between WT- and G503D-menin using cycloheximide stability assays (Figures S8C and S8D); similar results were observed in D418D (rs2071313) and A541T (rs2959656)

Table 2. Allele Frequency Distributions of Mutations (Polymorphisms) in *MEN1* Gene-Coding Regions of MDD Patients and Normal Controls

Position	SNP	m/M	Amino Acid Substitution	Case MAF	Control MAF	χ^2	OR	95% CI	p
64804659	rs375804228	C/T	G503D	0.013	0.004	7.236	3.208	1.37–7.50	0.00715
64804546	rs2959656	A/G	A541T	0.244	0.243	4.39E−4	1.002	0.85–1.17	0.983
64805130	rs2071313	T/C	D418D	0.420	0.421	0.001	0.996	0.81–1.22	0.972
64808033	rs607969	T/C		0.006	0.001	2.575	4.898	0.7–34.1	0.109
64805097	rs376598079	T/A/C		0.001	0	0.985	–	–	0.321
64805919	rs577726721	T/G		0	0.003	2.143	–	–	0.143
64804600	rs760683615	T/G		0.001	0	0.968	–	–	0.325
64804733	rs200280309	G/A		0.001	0.001	0.053	0.795	0.11–5.62	0.818
64806278	rs371364206	T/G		0.001	0	0.935	–	–	0.334

m/M, minor allele/major allele; MAF, minor allele frequency. p values were calculated by chi-square test.

constructs. Lastly, *MEN1* mutation had no effect on menin nuclear localization (Figure S8E). Together, these results indicate that rs375804228 (G503D) does not alter transcription, protein expression, protein turnover, or cellular localization profiles in menin.

Since menin associates with p65 to inhibit NF-κB transactivation, we speculated that G503D may affect menin-p65 association. Indeed, MEN1-G503D abolished menin-p65 interaction, with little or no effect on p65 localization (Figures 6A and S8F). Furthermore, MEN1-G503D mutation abrogated its ability to suppress p65-DNA binding interactions (Figure 6B). Although re-expression of WT-, D418D-, or A541T-menin could restore NF-κB-mediated transactivation in HEK293T cells transfected with *MEN1*-targeting small interfering RNAs, G503D mutation abolished rescue effects associated with menin re-expression (Figure 6C). Notably, elevations in NF-κB-mediated transactivation in *Men1*-deficient mouse astrocytes derived from cortex were reduced by MEN1-WT, -D418D, or -A541T expression, whereas G503D constructs failed to reduce NF-κB hyperactivity (Figure 6D). Furthermore, in human primary astrocytes, we also confirm that G503D menin mutant constructs failed to rescue NF-κB hyper-activation with *MEN1* downregulation with *shMEN1* expression (Figure 6E). Finally, elevations in IL-1β expression from *Men1*-deficient mouse astrocytes were reduced by MEN1-WT, -D418D, or -A541T expression; G503D constructs failed to reduce IL-1β overexpression (Figure 6F). Altogether, these results implicate a role for G503D MDD menin variants in abrogating menin-dependent suppression of NF-κB hyper-activation and pro-inflammatory IL-1β generation.

DISCUSSION

Neuroinflammation (Maes, 1994; Müller, 2014) and pathological alterations in astrocytic function (Slavich and Irwin, 2014; Wang et al., 2017) have been previously reported in depressive disorders. As the most abundant cell type in the brain, astrocytes play a central role in mediating and regulating neuroinflammation (Farina et al., 2007). However, molecular and cellular mechanisms underlying the regulation of astrocyte-mediated neuroinflammation in depression remain elusive. Here, we demonstrate that reduction of menin in astrocytes leads to a depressive-like phenotype, including despondent mood and social interactivity deficits. Increased neuroinflammation drives behavioral abnormalities in astroglial *Men1*-deficient mice. In addition, we identified a *MEN1* SNP, rs375804228, that is associated with an elevated risk of MDD onset and leads to aberrant NF-κB activation and IL-1β production.

Microglia and astrocytes mediate the production of pro-inflammatory cytokines (Brambilla et al., 2005; Farina et al., 2007), which drives the pathogenesis of depressive-like phenotypes (Fenn et al., 2014; Skaper et al., 2014). In the CNS, astrocytes represent the most abundant cell type in the brain and feature prominent NF-κB activity (Herkenham et al., 2011; Yang et al., 2009). Activation of NF-κB is a common feature in MDD and other neurological conditions (Caviedes et al., 2017), whereas NF-κB hyperactivity leads to the production of pro-inflammatory cytokines such as IL-1β, which is a key driver in the clinical manifestation of depressive symptoms. In addition to astrocytes, NF-κB is also expressed in microglia. Although our data directly indicate that NF-κB-mediated neuroinflammation in astrocytes results in depressive-like phenotypes, microglia may also similarly modulate neuroinflammation through NF-κB induction. Since menin levels are relatively low in microglia, the NF-κB pathway may be more sensitive to activation in microglia through menin-independent pathways. Furthermore, menin-deficient astrocyte-derived pro-inflammatory factors also induce microglial activation, thereby leading to neuronal dysfunction through numerous microglial-derived factors. Further, the sum of our results indicates that astrocyte-specific *Men1* deletion may be a useful model to study neuroinflammatory disorders.

Biological pathways mediated by pro-inflammatory cytokines in the pathogenesis of depression disorders include HPA (hypothalamic-pituitary-adrenal) axis dysfunction (Belvederi Murri et al., 2014; Krishnan and Nestler, 2008), reduced serotonin levels (Frodl et al., 2010; Gatt et al., 2009), and impaired neuroplasticity (Eyre and Baune, 2012; Yirmiya and Goshen, 2011). Glucocorticoids are generated, regulated, and secreted by the HPA axis, and are elevated in serum from patients suffering from depression (Parker et al., 2003; Raison and Miller, 2003). Further, serotonin levels were markedly decreased in *Men1*-deficient GcKO mice, while IL-1β-RA normalized serotonin levels (Figure 5G). Together, these results give strong indication that astrocytic menin can alter serotonin levels, which can have a visible impact on clinical depression.

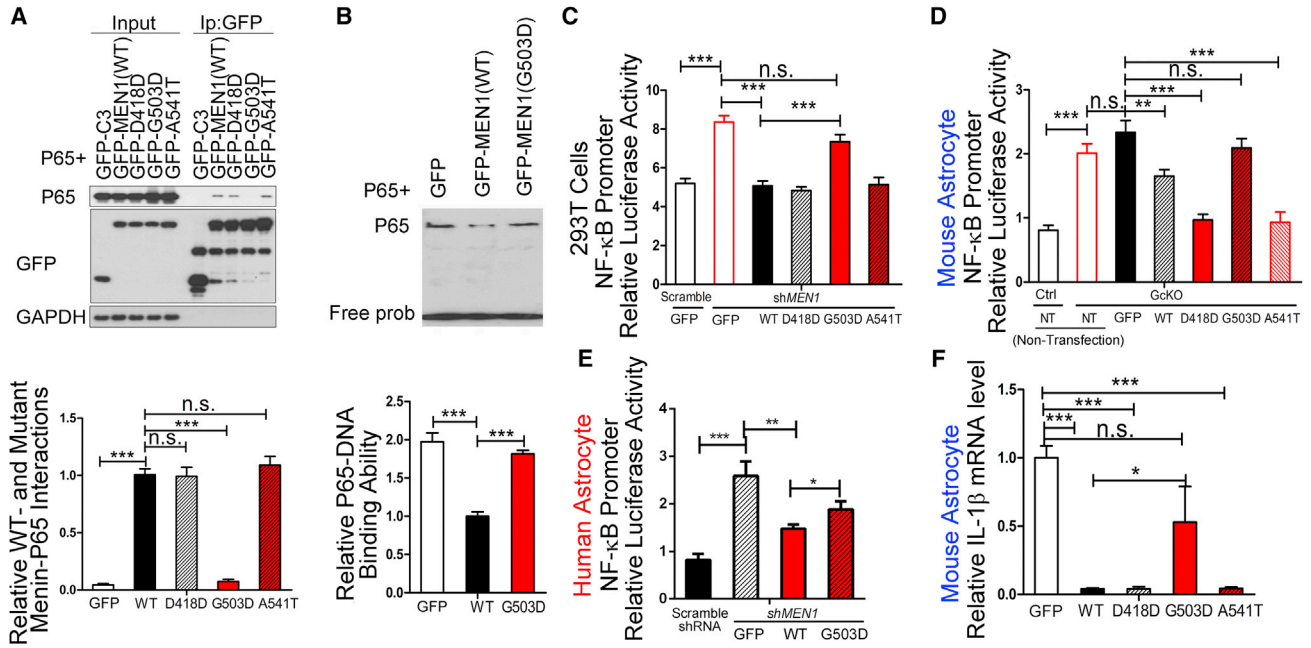

Figure 6. MDD-Associated G503D Menin Mutation Abrogates Menin/p65 Interactions and Menin-Dependent NF-κB Suppression

(A) Interactions between p65 and WT menin or relevant menin mutations were determined in HEK293T cells by co-transfection with p65 and GFP Ctrl, GFP-MEN1, GFP-MEN1-D418D, GFP-MEN1-G503D, or GFP-MEN1-A541T constructs. n = 3 experimental replicates/group. Quantification of p65/menin coprecipitation is presented in the graph below.

(B) p65 DNA binding activity measured by EMSA in HEK293T cells following transfection with the plasmids as indicated. n = 3 experimental replicates/group. Quantification is presented in the graph below.

(C) NFκB-mediated transactivation in HEK293T cells following transfection with plasmid vectors as indicated. n = 3 experimental replicates/group.

(D) NFκB-mediated transactivation in Ctrl or *Men1*-deficient astrocytes derived from mouse cortex transfected with vectors as indicated. n = 3 experimental replicates/group.

(E) NFκB-mediated transactivation in human primary astrocytes transfected with vectors as indicated. n = 3 experimental replicates/group.

(F) IL-1β levels in astrocytes derived from mouse cortex transfected with the vectors indicated as determined by ELISA. n = 4 experimental replicates/group.

Data represent mean ± SEM; n.s., not significant; *p < 0.05, **p < 0.01, ***p < 0.001, one-way ANOVA with Tukey's post hoc analysis.

See also Figure S8.

MDD was initially thought to be primarily triggered through neuronal dysfunction (Manji et al., 2001). Indeed, depression has been shown to be induced by dysregulated mechanisms that influence synaptic plasticity in afflicted regions (Duman and Aghajanian, 2012). Neuronal impairment in depression is associated with reduced dendritic complexity and spine number, as observed in postmortem brain samples from patients with depressive disorder and rodent stress models of depression (Rajkowska et al., 1999; Stockmeier et al., 2004). We observed a substantial decrease in dendritic complexity in the cortex and hippocampus of GcKO mice.

Although our study mainly concentrated on the two major brain areas of cortex and hippocampus, other brain regions are also associated with depression. The NAc plays key roles in depression symptomatology including anhedonia and reduced motivation (Lim et al., 2012; Stuber et al., 2011). We also observed that menin mRNA levels were markedly decreased in NAc of CUMS mouse brain, while IL-1β levels increased dramatically in NAc of GcKO mice (Figure S1). Since menin is expressed throughout the entire brain, the effect of menin on neuroinflammation in other brain regions warrants further investigation. Given that our results show that IL-1β-RA can restore morphogenic deficits and hippocampal LTP impairment, NF-κB inhibitors and IL-1β-RA may represent potential treatment strategies to ameliorate inflammation-based depression disorders.

Etiologically, MDD is a complex disease that involves a combination of environmental and genetic factors (Bosker et al., 2011). Cumulative evidence indicates that heritable genetic factors are associated with MDD (Hyde et al., 2016; Wray et al., 2012). Numerous candidate genes have been characterized in association with depression (Hyde et al., 2016) and functional links between depression and genes regulating the serotonin or neurotrophin signaling have been implicated (López-León et al., 2008; Nugent et al., 2011). Despite strong evidence supporting the involvement of heritable components in MDD, efforts to clarify biological mechanisms through common or rare variant association studies have been unsuccessful. This has been attributed to heterogeneity of the disease and absence of established standards in clinical diagnosis. Recently, genome-wide association studies have implicated several SNPs associated with major depression (Hek et al., 2013; Lewis et al., 2010; Nugent et al., 2011; Sullivan et al., 2009). The human *MEN1* gene is located at the 11q13.1 locus,

and *MEN1* gene mutations that normally inactivate this gene are commonly found in patients with MEN1 syndrome (Chandrasekharappa et al., 1997; Lemmens et al., 1997). To date, approximately 1,500 *MEN1* mutations have been reported in patients with endocrine disorders (Concolino et al., 2016; Lemos and Thakker, 2008); here, our results indicate that carriers of the *MEN1* SNP rs375804228 G503D risk variant are associated with a higher risk of MDD onset. This is the first *MEN1* gene mutation characterized outside of MEN1 syndrome and is unique among all *MEN1* gene mutations reported previously. The majority of MDD patients are heterozygous carriers for the rs375804228 SNP and would therefore be predicted to manifest a partial loss of menin function, thereby triggering consequent NF-κB activation/inflammation in depressive onset. Our findings linking this menin-associated SNP to MDD could be utilized in early diagnosis of depression through diagnostic screening and implicate potential attenuation of the NF-κB pathway in personalized treatment strategies in patients diagnosed with menin-associated MDD. Our data also indicate that MEN1 syndrome patients with *MEN1* mutations may also be at risk for MDD; future studies may indicate whether mutations associated with MEN1 syndrome can also affect MDD onset.

In summary, we have identified a distinct role for astrocytic menin in the onset of depression through neuroinflammatory pathways. These results also suggest that menin could also be a prognostic marker for depression disorders, which may be predictive of depressive symptoms and oncogenic potential.

STAR★METHODS

Detailed methods are provided in the online version of this paper and include the following:

- KEY RESOURCES TABLE
- CONTACT FOR REAGENT AND RESOURCE SHARING
- EXPERIMENTAL MODEL AND SUBJECT DETAILS
  - Human Subjects
  - Animals
- METHOD DETAILS
  - Experimental design
  - Drug Administration
  - Neuron, Astrocyte, Microglia, Oligodendrocyte and Tissue culture procedures
  - Western blotting
  - Quantitative RT-PCR
  - Plasmids and shRNA
  - NF-κB promoter-luciferase reporter assay
  - Golgi staining
  - Co-immunoprecipitation
  - Enzyme Linked Immunosorbent Assay (ELISA)
  - Electrophoretic Mobility Shift Assay (EMSA)
  - Immunofluorescence
  - Protein stability assays
  - Electrophysiology
  - *MEN1* coding regions sequencing
  - Behavioral Studies
  - RNA-Sequencing analysis
- QUANTIFICATION AND STATISTICAL ANALYSIS
  - Statistical analysis
  - Description of sample size (n-number)
- DATA AND SOFTWARE AVAILABILITY

SUPPLEMENTAL INFORMATION

Supplemental Information includes eight figures and can be found with this article online at https://doi.org/10.1016/j.neuron.2018.08.031.

ACKNOWLEDGMENTS

We thank Prof. Guanghui Jin (Xiamen University) and Prof. Xianxin Hua (University of Pennsylvania) for providing the Men1-floxp mice. This work was supported by the National Natural Science Foundation of China (grants 81522016, 81271421, and 31571055 to J.Z.; 81625008 and 31430048 to Q.X.; 81630026 to Z.Y.; 81771163 and U1405222 to H.X.; U1505227 to G.B.; 81472725 to W.M.), the Natural Science Foundation of Fujian Province of China (grant 2013J01147 and 2014J06019 to J.Z.), the Fundamental Research Funds for the Central Universities (grants 20720150062 and 20720180049 to J.Z.), the National Key Research and Development Program of China (2016YFC1305903), and CAMS Innovation Fund for Medical Sciences (grant 2016I2M1004 to Q.X.).

AUTHOR CONTRIBUTIONS

L.L. and J.Z. conceptualized the study; L.L., K. Zhuang, C.H., H. Lin, and Y.H. prepared and maintained *Men1* cKO mice; L.L., K. Zhuang, and Y.G. designed and performed morphological analysis and biochemical assays; L.L., K. Zhuang, Y.G., and G.C. performed behavior tests; and Y.G. performed electrophysiology experiments and Golgi staining. H.S. supervised the electrophysiology experiments. K. Zhang and W.M. performed the oligodendrocyte experiments. Z.L. and Q.X. performed and analyzed MDD patient SNPs; Z.S. performed the human astrocyte experiments; and D.W., M.S., W.X., and H. Li prepared materials. G.C. and H. Lin prepared primary neuronal cultures. L.L. and J.Z. wrote the manuscript. T.Y.H., X.Z., Z.Y., M.X., H.X., and G.B. discussed and edited the manuscript. J.Z. supervised the project. All authors reviewed and gave final approval to the manuscript.

DECLARATION OF INTERESTS

The authors declare no competing interests.

Received: April 22, 2018
Revised: July 4, 2018
Accepted: August 21, 2018
Published: September 13, 2018

REFERENCES

Akbarian, S., Rios, M., Liu, R.J., Gold, S.J., Fong, H.F., Zeiler, S., Coppola, V., Tessarollo, L., Jones, K.R., Nestler, E.J., et al. (2002). Brain-derived neurotrophic factor is essential for opiate-induced plasticity of noradrenergic neurons. J. Neurosci. *22*, 4153–4162.

Allen, N.J. (2014). Astrocyte regulation of synaptic behavior. Annu. Rev. Cell Dev. Biol. *30*, 439–463.

Aoki, A., Tsukada, T., Yasuda, H., Kayashima, S., Nagase, T., Ito, T., Suzuki, T., Matsukuma, S., Kuwabara, N., Yoshimoto, K., and Yamaguchi, K. (1997). Multiple endocrine neoplasia type 1 presented with manic-depressive disorder: a case report with an identified MEN1 gene mutation. Jpn. J. Clin. Oncol. *27*, 419–422.

Baltimore, D. (2011). NF-κB is 25. Nat. Immunol. *12*, 683–685.

Bazzi, W., Renon, M., Vercherat, C., Hamze, Z., Lacheretz-Bernigaud, A., Wang, H., Blanc, M., Roche, C., Calender, A., Chayvialle, J.A., et al. (2008). MEN1 missense mutations impair sensitization to apoptosis induced by wild-type menin in endocrine pancreatic tumor cells. Gastroenterology *135*, 1698–1709.e2.

Belvederi Murri, M., Pariante, C., Mondelli, V., Masotti, M., Atti, A.R., Mellacqua, Z., Antonioli, M., Ghio, L., Menchetti, M., Zanetidou, S., et al. (2014). HPA axis and aging in depression: systematic review and meta-analysis. Psychoneuroendocrinology *41*, 46–62.

Bosker, F.J., Hartman, C.A., Nolte, I.M., Prins, B.P., Terpstra, P., Posthuma, D., van Veen, T., Willemsen, G., DeRijk, R.H., de Geus, E.J., et al. (2011). Poor replication of candidate genes for major depressive disorder using genome-wide association data. Mol. Psychiatry *16*, 516–532.

Brambilla, R., Bracchi-Ricard, V., Hu, W.H., Frydel, B., Bramwell, A., Karmally, S., Green, E.J., and Bethea, J.R. (2005). Inhibition of astroglial nuclear factor kappaB reduces inflammation and improves functional recovery after spinal cord injury. J. Exp. Med. *202*, 145–156.

Can, A., Dao, D.T., Terrillion, C.E., Piantadosi, S.C., Bhat, S., and Gould, T.D. (2012). The tail suspension test. J. Vis. Exp. e3769.

Canaff, L., Vanbellinghen, J.F., Kanazawa, I., Kwak, H., Garfield, N., Vautour, L., and Hendy, G.N. (2012). Menin missense mutants encoded by the MEN1 gene that are targeted to the proteasome: restoration of expression and activity by CHIP siRNA. J. Clin. Endocrinol. Metab. *97*, E282–E291.

Canals, J., Carbajo, G., and Fernández-Ballart, J. (2002). Discriminant validity of the Eating Attitudes Test according to American Psychiatric Association and World Health Organization criteria of eating disorders. Psychol. Rep. *91*, 1052–1056.

Castrén, E. (2013). Neuronal network plasticity and recovery from depression. JAMA Psychiatry *70*, 983–989.

Caviedes, A., Lafourcade, C., Soto, C., and Wyneken, U. (2017). BDNF/NF-κB signaling in the neurobiology of depression. Curr. Pharm. Des. *23*, 3154–3163.

Chandrasekharappa, S.C., Guru, S.C., Manickam, P., Olufemi, S.E., Collins, F.S., Emmert-Buck, M.R., Debelenko, L.V., Zhuang, Z., Lubensky, I.A., Liotta, L.A., et al. (1997). Positional cloning of the gene for multiple endocrine neoplasia-type 1. Science *276*, 404–407.

Chatterjee, M., Jaiswal, M., and Palit, G. (2012). Comparative evaluation of forced swim test and tail suspension test as models of negative symptom of schizophrenia in rodents. ISRN Psychiatry *2012*, 595141.

Christoffel, D.J., Golden, S.A., and Russo, S.J. (2011). Structural and synaptic plasticity in stress-related disorders. Rev. Neurosci. *22*, 535–549.

Cogswell, J.P., Godlevski, M.M., Wisely, G.B., Clay, W.C., Leesnitzer, L.M., Ways, J.P., and Gray, J.G. (1994). NF-kappa B regulates IL-1 beta transcription through a consensus NF-kappa B binding site and a nonconsensus CRE-like site. J. Immunol. *153*, 712–723.

Concolino, P., Costella, A., and Capoluongo, E. (2016). Multiple endocrine neoplasia type 1 (MEN1): An update of 208 new germline variants reported in the last nine years. Cancer Genet. *209*, 36–41.

CONVERGE consortium (2015). Sparse whole-genome sequencing identifies two loci for major depressive disorder. Nature *523*, 588–591.

Crabtree, J.S., Scacheri, P.C., Ward, J.M., McNally, S.R., Swain, G.P., Montagna, C., Hager, J.H., Hanahan, D., Edlund, H., Magnuson, M.A., et al. (2003). Of mice and MEN1: insulinomas in a conditional mouse knockout. Mol. Cell. Biol. *23*, 6075–6085.

Duman, R.S., and Aghajanian, G.K. (2012). Synaptic dysfunction in depression: potential therapeutic targets. Science *338*, 68–72.

Eyre, H., and Baune, B.T. (2012). Neuroplastic changes in depression: a role for the immune system. Psychoneuroendocrinology *37*, 1397–1416.

Fang, M., Xia, F., Mahalingam, M., Virbasius, C.M., Wajapeyee, N., and Green, M.R. (2013). MEN1 is a melanoma tumor suppressor that preserves genomic integrity by stimulating transcription of genes that promote homologous recombination-directed DNA repair. Mol. Cell. Biol. *33*, 2635–2647.

Farina, C., Aloisi, F., and Meinl, E. (2007). Astrocytes are active players in cerebral innate immunity. Trends Immunol. *28*, 138–145.

Fenn, A.M., Gensel, J.C., Huang, Y., Popovich, P.G., Lifshitz, J., and Godbout, J.P. (2014). Immune activation promotes depression 1 month after diffuse brain injury: a role for primed microglia. Biol. Psychiatry *76*, 575–584.

Ferrari, A.J., Charlson, F.J., Norman, R.E., Patten, S.B., Freedman, G., Murray, C.J., Vos, T., and Whiteford, H.A. (2013). Burden of depressive disorders by country, sex, age, and year: findings from the global burden of disease study 2010. PLoS Med. *10*, e1001547.

Frodl, T., Reinhold, E., Koutsouleris, N., Donohoe, G., Bondy, B., Reiser, M., Möller, H.J., and Meisenzahl, E.M. (2010). Childhood stress, serotonin transporter gene and brain structures in major depression. Neuropsychopharmacology *35*, 1383–1390.

Gang, D., Hongwei, H., Hedai, L., Ming, Z., Qian, H., and Zhijun, L. (2013). The tumor suppressor protein menin inhibits NF-κB-mediated transactivation through recruitment of Sirt1 in hepatocellular carcinoma. Mol. Biol. Rep. *40*, 2461–2466.

Gatt, J.M., Nemeroff, C.B., Dobson-Stone, C., Paul, R.H., Bryant, R.A., Schofield, P.R., Gordon, E., Kemp, A.H., and Williams, L.M. (2009). Interactions between BDNF Val66Met polymorphism and early life stress predict brain and arousal pathways to syndromal depression and anxiety. Mol. Psychiatry *14*, 681–695.

Gimelli, S., Makrythanasis, P., Stouder, C., Antonarakis, S.E., Bottani, A., and Béna, F. (2011). A de novo 12q13.11 microdeletion in a patient with severe mental retardation, cleft palate, and high myopia. Eur. J. Med. Genet. *54*, 94–96.

Gross, M., and Pinhasov, A. (2016). Chronic mild stress in submissive mice: Marked polydipsia and social avoidance without hedonic deficit in the sucrose preference test. Behav. Brain Res. *298* (Pt B), 25–34.

Hek, K., Demirkan, A., Lahti, J., Terracciano, A., Teumer, A., Cornelis, M.C., Amin, N., Bakshis, E., Baumert, J., Ding, J., et al. (2013). A genome-wide association study of depressive symptoms. Biol. Psychiatry *73*, 667–678.

Heppner, C., Bilimoria, K.Y., Agarwal, S.K., Kester, M., Whitty, L.J., Guru, S.C., Chandrasekharappa, S.C., Collins, F.S., Spiegel, A.M., Marx, S.J., and Burns, A.L. (2001). The tumor suppressor protein menin interacts with NF-kappaB proteins and inhibits NF-kappaB-mediated transactivation. Oncogene *20*, 4917–4925.

Herkenham, M., Rathore, P., Brown, P., and Listwak, S.J. (2011). Cautionary notes on the use of NF-κB p65 and p50 antibodies for CNS studies. J. Neuroinflammation *8*, 141.

Hyde, C.L., Nagle, M.W., Tian, C., Chen, X., Paciga, S.A., Wendland, J.R., Tung, J.Y., Hinds, D.A., Perlis, R.H., and Winslow, A.R. (2016). Identification of 15 genetic loci associated with risk of major depression in individuals of European descent. Nat. Genet. *48*, 1031–1036.

Koo, J.W., and Duman, R.S. (2009). Evidence for IL-1 receptor blockade as a therapeutic strategy for the treatment of depression. Curr. Opin. Investig. Drugs *10*, 664–671.

Krishnan, V., and Nestler, E.J. (2008). The molecular neurobiology of depression. Nature *455*, 894–902.

Lemmens, I., Van de Ven, W.J., Kas, K., Zhang, C.X., Giraud, S., Wautot, V., Buisson, N., De Witte, K., Salandre, J., Lenoir, G., et al. (1997). Identification of the multiple endocrine neoplasia type 1 (MEN1) gene. The European Consortium on MEN1. Hum. Mol. Genet. *6*, 1177–1183.

Lemos, M.C., and Thakker, R.V. (2008). Multiple endocrine neoplasia type 1 (MEN1): analysis of 1336 mutations reported in the first decade following identification of the gene. Hum. Mutat. *29*, 22–32.

Lewis, C.M., Ng, M.Y., Butler, A.W., Cohen-Woods, S., Uher, R., Pirlo, K., Weale, M.E., Schosser, A., Paredes, U.M., Rivera, M., et al. (2010). Genome-wide association study of major recurrent depression in the U.K. population. Am. J. Psychiatry *167*, 949–957.

Lim, B.K., Huang, K.W., Grueter, B.A., Rothwell, P.E., and Malenka, R.C. (2012). Anhedonia requires MC4R-mediated synaptic adaptations in nucleus accumbens. Nature *487*, 183–189.

López-León, S., Janssens, A.C., González-Zuloeta Ladd, A.M., Del-Favero, J., Claes, S.J., Oostra, B.A., and van Duijn, C.M. (2008). Meta-analyses of genetic studies on major depressive disorder. Mol. Psychiatry *13*, 772–785.

Maes, M. (1994). Cytokines in major depression. Biol. Psychiatry *36*, 498–499.

Manji, H.K., Drevets, W.C., and Charney, D.S. (2001). The cellular neurobiology of depression. Nat. Med. *7*, 541–547.

Mao, X.R., Moerman-Herzog, A.M., Chen, Y., and Barger, S.W. (2009). Unique aspects of transcriptional regulation in neurons–nuances in NFkappaB and Sp1-related factors. J. Neuroinflammation *6*, 16.

Matkar, S., Thiel, A., and Hua, X. (2013). Menin: a scaffold protein that controls gene expression and cell signaling. Trends Biochem. Sci. *38*, 394–402.

Müller, N. (2014). Immunology of major depression. Neuroimmunomodulation *21*, 123–130.

Norman, G.J., Karelina, K., Zhang, N., Walton, J.C., Morris, J.S., and Devries, A.C. (2010). Stress and IL-1beta contribute to the development of depressive-like behavior following peripheral nerve injury. Mol. Psychiatry *15*, 404–414.

Nugent, N.R., Tyrka, A.R., Carpenter, L.L., and Price, L.H. (2011). Gene-environment interactions: early life stress and risk for depressive and anxiety disorders. Psychopharmacology (Berl.) *214*, 175–196.

Oeckinghaus, A., and Ghosh, S. (2009). The NF-kappaB family of transcription factors and its regulation. Cold Spring Harb. Perspect. Biol. *1*, a000034.

Parker, K.J., Schatzberg, A.F., and Lyons, D.M. (2003). Neuroendocrine aspects of hypercortisolism in major depression. Horm. Behav. *43*, 60–66.

Parker, M., Mohankumar, K.M., Punchihewa, C., Weinlich, R., Dalton, J.D., Li, Y., Lee, R., Tatevossian, R.G., Phoenix, T.N., Thiruvenkatam, R., et al. (2014). C11orf95-RELA fusions drive oncogenic NF-κB signalling in ependymoma. Nature *506*, 451–455.

Raison, C.L., and Miller, A.H. (2003). When not enough is too much: the role of insufficient glucocorticoid signaling in the pathophysiology of stress-related disorders. Am. J. Psychiatry *160*, 1554–1565.

Rajkowska, G., and Stockmeier, C.A. (2013). Astrocyte pathology in major depressive disorder: insights from human postmortem brain tissue. Curr. Drug Targets *14*, 1225–1236.

Rajkowska, G., Miguel-Hidalgo, J.J., Wei, J., Dilley, G., Pittman, S.D., Meltzer, H.Y., Overholser, J.C., Roth, B.L., and Stockmeier, C.A. (1999). Morphometric evidence for neuronal and glial prefrontal cell pathology in major depression. Biol. Psychiatry *45*, 1085–1098.

Rivers, L.E., Young, K.M., Rizzi, M., Jamen, F., Psachoulia, K., Wade, A., Kessaris, N., and Richardson, W.D. (2008). PDGFRA/NG2 glia generate myelinating oligodendrocytes and piriform projection neurons in adult mice. Nat. Neurosci. *11*, 1392–1401.

Sanacora, G., and Banasr, M. (2013). From pathophysiology to novel antidepressant drugs: glial contributions to the pathology and treatment of mood disorders. Biol. Psychiatry *73*, 1172–1179.

Scacheri, P.C., Crabtree, J.S., Kennedy, A.L., Swain, G.P., Ward, J.M., Marx, S.J., Spiegel, A.M., and Collins, F.S. (2004). Homozygous loss of menin is well tolerated in liver, a tissue not affected in MEN1. Mamm. Genome *15*, 872–877.

Skaper, S.D., Facci, L., and Giusti, P. (2014). Neuroinflammation, microglia and mast cells in the pathophysiology of neurocognitive disorders: a review. CNS Neurol. Disord. Drug Targets *13*, 1654–1666.

Slavich, G.M., and Irwin, M.R. (2014). From stress to inflammation and major depressive disorder: a social signal transduction theory of depression. Psychol. Bull. *140*, 774–815.

Stockmeier, C.A., Mahajan, G.J., Konick, L.C., Overholser, J.C., Jurjus, G.J., Meltzer, H.Y., Uylings, H.B., Friedman, L., and Rajkowska, G. (2004). Cellular changes in the postmortem hippocampus in major depression. Biol. Psychiatry *56*, 640–650.

Stuber, G.D., Sparta, D.R., Stamatakis, A.M., van Leeuwen, W.A., Hardjoprajitno, J.E., Cho, S., Tye, K.M., Kempadoo, K.A., Zhang, F., Deisseroth, K., and Bonci, A. (2011). Excitatory transmission from the amygdala to nucleus accumbens facilitates reward seeking. Nature *475*, 377–380.

Sullivan, P.F., de Geus, E.J., Willemsen, G., James, M.R., Smit, J.H., Zandbelt, T., Arolt, V., Baune, B.T., Blackwood, D., Cichon, S., et al. (2009). Genome-wide association for major depressive disorder: a possible role for the presynaptic protein piccolo. Mol. Psychiatry *14*, 359–375.

Tronche, F., Kellendonk, C., Kretz, O., Gass, P., Anlag, K., Orban, P.C., Bock, R., Klein, R., and Schütz, G. (1999). Disruption of the glucocorticoid receptor gene in the nervous system results in reduced anxiety. Nat. Genet. *23*, 99–103.

Trumpp, A., Depew, M.J., Rubenstein, J.L., Bishop, J.M., and Martin, G.R. (1999). Cre-mediated gene inactivation demonstrates that FGF8 is required for cell survival and patterning of the first branchial arch. Genes Dev. *13*, 3136–3148.

Wang, Q., Jie, W., Liu, J.H., Yang, J.M., and Gao, T.M. (2017). An astroglial basis of major depressive disorder? An overview. Glia *65*, 1227–1250.

Westerman, B.A., Blom, M., Tanger, E., van der Valk, M., Song, J.Y., van Santen, M., Gadiot, J., Cornelissen-Steijger, P., Zevenhoven, J., Prosser, H.M., et al. (2012). GFAP-Cre-mediated transgenic activation of Bmi1 results in pituitary tumors. PLoS ONE *7*, e35943.

Wray, N.R., Pergadia, M.L., Blackwood, D.H., Penninx, B.W., Gordon, S.D., Nyholt, D.R., Ripke, S., MacIntyre, D.J., McGhee, K.A., Maclean, A.W., et al. (2012). Genome-wide association study of major depressive disorder: new results, meta-analysis, and lessons learned. Mol. Psychiatry *17*, 36–48.

Yang, K., Xie, G.R., Hu, Y.Q., Mao, F.Q., and Su, L.Y. (2009). Association study of astrocyte-derived protein S100B gene polymorphisms with major depressive disorder in Chinese people. Can. J. Psychiatry *54*, 312–319.

Yirmiya, R., and Goshen, I. (2011). Immune modulation of learning, memory, neural plasticity and neurogenesis. Brain Behav. Immun. *25*, 181–213.

Zhuang, K., Huang, C., Leng, L., Zheng, H., Gao, Y., Chen, G., Ji, Z., Sun, H., Hu, Y., Wu, D., et al. (2018). Neuron-specific menin deletion leads to synaptic dysfuntion and cognitive impairment by modulating p35 expression. Cell Rep. *24*, 701–712.

STAR★METHODS

KEY RESOURCES TABLE

REAGENT or RESOURCE	SOURCE	IDENTIFIER
Antibodies		
menin	Abcam	# Ab4452; RRID: AB_304464
p65	Cell Signaling Technology	#8242; RRID: AB_10859369
Tuj1	Abcam	#Ab2276-1; RRID: AB_1267370
NR2A	Cell Signaling Technology	# 4205S; RRID: AB_2112295
NR2B	Cell Signaling Technology	# 4207S; RRID: AB_1264223
GluR1	LifeSpan	#LS-C23869-100; RRID: AB_900898
GFAP	Cell Signaling Technology	#3670; RRID: AB_561049
NeuN	Millipore	#MAB377; RRID: AB_2298772
PSD95	Abcam	#Ab12093; RRID: AB_298846
CC1	Millipore	#OP80; RRID: AB_2057371
PDGFRα	R&D	#AF1062; RRID: AB_2236897
MBP	Santacruz	#Sc13914; RRID: AB_648798
GFAP	Santacruz	#Sc6170; RRID: AB_641021
Synaptophysin	Sigma	#SAB4502906; RRID: AB_10746692
IBA1	Santacruz	#Sc-32725; RRID: AB_667733
Synapsin I	Abcam	# Ab1543; RRID: AB_2200400
GAPDH	Abcam	#Ab9485; RRID: AB_307275
HnRNP	Santacruz	#Sc-32301; RRID: AB_627729
Biological Samples		
DNA from MDD and control patients	This paper	First Hospital of Shanxi Medical University, Taiyuan, China; 014-2016
Chemicals, Peptides, and Recombinant Proteins		
Interleukin-1 receptor antagonist	BBI Life Sciences	#RC003
PDTC	Beyotime	#S1808
Tamoxifin	Sigma	#T5648
LPS	Sigma	#L4130
Deposited Data		
RNA Seq	This paper	SRA: SRP151969
Experimental Models: Organisms/Strains		
Men1$^{floxp/floxp}$	The Jackson Laboratory	JAX: 005109
Nestin-Cre	The Jackson Laboratory	JAX:003173
CamKIIα-Cre	The Jackson Laboratory	JAX: 005359
GFAP-Cre	The Jackson Laboratory	JAX:024098
Fgfr3-icreER	The Jackson Laboratory	JAX:025809
Oligonucleotides		
Men1shRNA	This paper	N/A
Primer for RT-PCR, see table in Quantitative RT-PCR	This paper	N/A
Primer for plasmid construction, see table in Plasmids and shRNA	This paper	N/A
Recombinant DNA		
pEGFP-C3-MEN1	This paper	N/A
pEGFP-C3-MEN1(D418D)	This paper	N/A
pEGFP-C3-MEN1(G503D)	This paper	N/A

(*Continued on next page*)

Continued

REAGENT or RESOURCE	SOURCE	IDENTIFIER
pEGFP-C3-MEN1(A541T)	This paper	N/A
pEGFP-C3-NES-MEN1	This paper	N/A
pEGFP-C3-MEN1-277∼541	This paper	N/A
Software and Algorithms		
Labview	National Instruments	http://www.ni.com/en-us.html
MATLAB	MathWorks	https://www.mathworks.com
GraphPad Prism version 5.0	GraphPad Software	https://www.graphpad.com/
Lasergene software (version 7.1)	DNASTAR	http://www.dnastar.com

CONTACT FOR REAGENT AND RESOURCE SHARING

Further information and requests for resources and reagents should be directed to and will be fulfilled by the Lead Contact, Jie Zhang (jiezhang@xmu.edu.cn).

EXPERIMENTAL MODEL AND SUBJECT DETAILS

Human Subjects

A total of 1032 unrelated patients with MDD (439 males and 593 females) were recruited from the Department of Psychiatry, First Hospital of Shanxi Medical University, Taiyuan, China; at time period between January 2006 and December 2013. Clinical diagnosis was assessed by a minimum of two psychiatrists according to criteria established by the "Diagnostic and Statistical Manual of Mental Disorders Fourth Edition (DSM-IV)" for major depressive disorders. Cases comprised an age range of 37.0 ± 13.59 (SD) years, and experienced at least one episode of MDD within established DSM-IV clinical criteria. Criteria to exclude patients within our analyses include pre-existing history of bipolar disorder, mental retardation, psychosis, severe medical conditions, pregnancy, abnormal laboratory baseline values, and/or a history of alcoholism or drug abuse. Meanwhile, 866 unrelated healthy subjects (381 males and 485 females), were also recruited as controls. Controls were recruited from local communities and information was disclosed regarding medical and family history. Controls comprised ages ranging 40.86 ± 14.06 (SD) years. Criteria to exclude patients within the control group include a history of major psychiatric or neurological disorders, psychiatric treatment or drug abuse, and/or family history of inherited severe psychiatric disorder. MDD and control subjects were respectively stratified into six subsets according to their age (< 21; 21-30, 31-40, 41-50, 51-60 and > 60). 40% of the individuals were randomly sampled from each subset for analysis. All the subjects were of Chinese Han origin, and originated from Northern China. Detailed clinical information regarding the patients and controls are presented in Table 1. Written informed consents were obtained from all patients and controls in this study, and approved by the Ethics Committee of Chinese Academy of Medical Sciences and Peking Union Medical College (014-2016).

Animals

All mice were maintained in the core animal facility at Xiamen University, and all experimental procedures involved were performed according to protocols approved by the Institutional Animal Care and Use Committee at Xiamen University.

Mice were housed under a 12 h light/dark cycle with free access to standard rodent chow and water. Each cage housed a maximum of four mice. Mice were maintained under Specific-Pathogen-Free (SPF) conditions and were not subject to immunosuppression. Health of the animals used was regularly controlled by animal caretakers. All mice used in the study were not previously involved in other experimental procedures, and were free from other non-relevant exposure to drugs or tests. A mixture of 2 month old litter/age-matched male and female mice were employed in all studies and no differences between sexes were observed. Animals were used according to "3Rs" principles (Replacement, Reduction and Refinement) in all experimental procedures. In some experiments, animals were subjected to two experimental conditions with a single control group (Figures 4F and 4G) to minimize the number of animals used.

The floxed *Men1* mouse strain was obtained from Dr. Guanghui Jin and Dr. Xianxin Hua (Crabtree et al., 2003). *Nestin-Cre*, *CamkII*α*-cre*, *GFAP-Cre* and *Fgfr3-iCre(ER)* transgenic mice (Scacheri et al., 2004; Tronche et al., 1999; Trumpp et al., 1999; Westerman et al., 2012) were obtained from Dr. Jiawei Zhou at the Institute of Neuroscience, Chinese Academy of Science; these mice are available from Jackson Laboratory. *Men1*-NcKO, CcKO, GcKO and FcKO mice were obtained by crossing *Men1* floxed mice with respective *Nestin-Cre*, *CamkII*α*-cre*, *GFAP-Cre* or *Fgfr3-iCre(ER)* mouse lines. *Men1* floxed mice were used as controls. FcKO or control mice were treated with tamoxifin at 0.2 mg/g body weight or vehicle control by oral gavage once a day for five consecutive days. Tamoxifin was dissolved in 5% ethanol/corn oil at a final concentration of 50 mg/mL.

Chronic Unpredictable Mild Stress (CUMS): C57BL/6 male wild-type mice were divided into control and CUMS groups. CUMS mice were maintained in individual cages. CUMS involved exposure to a variety of mild stressors: (i) 24h food deprivation, (ii) 24h water deprivation, (iii) 1h of exposure to an empty bottle, (iv) 7h cage tilt (45°), (v) overnight illumination, (vi) 24h habitation in a soiled

cage (200 mL of water in 100 g of sawdust bedding), (vii) 30 min of forced swimming at 8°C, (viii) 2h of physical restraint, and (ix) 24h of exposure to a foreign object (e.g., a piece of plastic). These stressors were randomly scheduled over a 3 week period.

LPS-induced mouse model: Male C57BL6/J mice (2 months) were intraperitoneally injected with LPS (Sigma, L-2880) dissolved in sterile 0.9% saline at 0.5mg/kg. This dosage was used to stimulate infection without inducing obvious inflammation or other maladies. Saline or LPS injection was administered between 09:00 and 09:30 a.m. daily for 10 days. Behavioral tests were performed 24 hours following the last injection. Brain tissue and serum was dissected/sampled 24h following behavioral testing for western blotting and ELISA experiments.

METHOD DETAILS

Experimental design

All experiments described in this study were performed a minimum of 3 times. We did not use a statistical method to predetermine the proper sample size. The sample size per experiment was determined according to previous publications. All the experiments involving cKO mice and relevant rescue experiments were performed and analyzed in a blind manner. Specifically, mouse genotype was de-identified during the experimental trials in the behavioral analyses described. Similarly, mice subjected to electrophysiological analysis (LTP) were identified by number where the genotype was withheld during electrophysiological recording. In our image analysis for neuronal morphology, images were acquired and genotype/treatment was de-identified in the image files for analysis.

Drug Administration

IL-1β-RA (BBI Life Sciences #RC003) was dissolved in aCSF and applied to slice preparations for electrophysiological analysis by perfusion at a final concentration of 200 μg/μl. For behavioral analysis, PDTC and IL-1β-RA were dissolved in 0.9% NaCl and administered intraperitoneally at 50 mg/kg and 50 pg/kg, respectively.

Neuron, Astrocyte, Microglia, Oligodendrocyte and Tissue culture procedures

Primary neurons were dissected from timed-pregnant females at E16.5. Briefly, brain cortices were dissected from pups of varying genotypes. The meninges were removed, and cortical tissue was dissociated by enzymatic digestion. Isolated primary neurons were plated on poly-D-lysine coated dishes, and cultured in Neurobasal medium supplemented with B27 (GIBCO)/1% penicillin/streptomycin (Invitrogen) and maintained in a 5% CO_2 incubator at 37°C.

Primary astrocytes were cultured in astroglial medium (Dulbecco's modified eagle medium/Nutrient mixture F-12 (DMEM/F12) (1:1) (GIBCO) with 10% fetal bovine serum (FBS). Contaminating cells in the astroglia monolayer were removed by overnight shaking at 220 rpm at 37°C. For co-culture experiments, astroglial cells were seeded on matrigel-coated cell culture inserts (Costar, #3450, #3470) and transferred to DIV1 primary neurons. 5 μM AraC was supplemented to reduce glial proliferation. Co-cultures were maintained for 10 days before immunostaining or western blotting. Three independent cultures were generated and analyzed for all experiments. Human primary astrocytes were purchased from ScienCell (HA1800) and cultured in Astrocyte Medium (ScienCell, #1801). Human astrocytes were electroporated using a Lonza nucleofector with an Amaxa Basic Nucleofector Kit according to the manufacturer's instructions.

Primary microglial cultures were obtained by microdissection from brains of <2-day-old neonatal C57BL/6J mice. After removing the meninges, brains were mechanically minced and dissociated with 0.25% trypsin. After trypsin inactivation, the tissue suspension was passed through a 70 μm nylon cell strainer. Cell pellets were harvested and resuspended in DMEM supplemented with 10% heat-inactivated FBS and plated on poly-L-lysine pre-coated culture flasks. After 3 days, medium was changed, containing 25 ng/mL GM-CSF and 10% FBS. Primary microglial cells were harvested by shaking (200 rpm, 20 min) after 10-12d in culture, and every 3 days thereafter.

Mouse oligodendrocyte precursor cells (OPCs) were isolated from P4 to P7 mouse brain cortices. Briefly, dissociated mouse cortices were resuspended in panning buffer. The cells were incubated on panning plates coated with an anti-GalC antibody for 30 min to deplete mature oligodendrocytes, and subsequently incubated for 45 min on panning plates coated with an anti-O4 antibody to collect OPCs. Adherent cells were trypsinized and seeded onto poly-D-lysine-coated plates. Cells were grown in serum-free media with 2% B-27, 1% N2, PDGF-AA (20 ng/mL), bFGF (20 ng/mL), CNTF (10 ng/mL) and NT3 (1 ng/mL). OPC differentiation was induced by the removal of PDGF-AA, bFGF and NT3 from the growth media, and triiodothyronine (T3) (60 nM) was added to the cultures.

HEK293T, CHG5-MEN1 and CHG cell lines were cultured in DMEM supplemented with 10% FBS and maintained at 37°C in humidified air containing 5% CO_2. A stable menin-overexpressing cell line CHG5-MEN1 was established in a CHG human glioma cell line.

Western blotting

Cultured cells and mouse brain tissues (include cortex and hippocampus) were homogenized in lysis buffer (RIPA) on ice for 40 min, and subsequently centrifuged at 12,000 rpm for 10 min at 4°C. Supernatants were transferred to a clean 1.5ml tube and protein samples were resolved by SDS-PAGE (sodium dodecyl sulfate–polyacrylamide gel electrophoresis) and subsequent immunoblotted onto PVDF membranes. Sample containing 30 μg of protein was separated using 10% SDS-PAGE gels. Proteins were transferred onto PVDF (polyvinylidene difluoride) membranes in an ice cold buffer (25 mM Tris HCl, 192 mM glycine, and 20% methanol) by electrotransfer for 1.5 h. Immunoblots were probed with indicated antibodies. Goat-anti-mouse secondary antibodies and goat-anti-rabbit

secondary antibody were purchased from Millipore (#AP132P, #AP124P). Quantification of band intensities were normalized to β-actin or GAPDH (in total protein or cytoplasmic extract) or hnRNP (for nuclear extracts), and averaged from at least three independent experiments.

Quantitative RT-PCR

Total RNA from animal tissues and cells were isolated using Trizol reagent according to the manufacturer's instructions (Invitrogen). Reverse transcription was performed using ReverTra Ace qPCR RT Master Mix (Toyobo, FSQ-201). RNA concentrations were adjusted to 1.2 μg/μL in nuclease-free water, and total RNA was reverse-transcribed in a 20 μL reaction volume. cDNA was amplified by real-time quantitative RT-PCR using SYBR Green (Roche) reagent. Samples were assayed in triplicate and GAPDH was used as an internal control. Primer sequences used for qPCR and in this study are as follows:

Gene	Primer sequences
MEN1	Forward 5′-ACCTATCCATCATTGCTGCCCTCT-3′
	Reverse5′-ACCAGTTCGCGACTAGAAACACCT-3′
GAPDH	Forward 5′-AGGTCGGTGTGAACGGATTTG-3′
	Reverse5′-TGTAGACCATGTAGTTGAGGTCA-3′
COX-2	Forward 5′-CCCTGCTGCCCGACACCTTC-3′
	Reverse5′-CCAGCAACCCGGCCAGCAAT-3′
IL-2	Forward 5′-CGCACCCACTTCAAGCTCCACTTC-3′
	Reverse5′-ATTCTGTGGCCTGCTTGGGCAAG-3′
IL-12β	Forward 5′-TGGTTTGCCATCGTTTTGCTG-3′
	Reverse5′-ACAGGTGAGGTTCACTGTTTCT-3′
INF-γ	Forward 5′-GGCTGTTACTGCCACGGCACA-3′
	Reverse5′-CACCATCCTTTTGCCAGTTCCTCCA-3′
IL-1β	Forward 5′-ATGGCAACTGTTCCTGAACTCAACT-3′
	Reverse5′-CAGGACAGGTATAGATTCTTTCCTTT-3′
IL-6	Forward 5′-TCCAGTTGCCTTCTTGGGAC-3′
	Reverse5′-GTGTAATTAAGCCTCCGACTTG-3′
TGF-α	Forward5′-TTCTGTCTACTGAACTTCGGGGTGATCGGTCC-3′
	Reverse5′-GTATGAGATAGCAAATCGGCTGACGGTGTGGG-3′
NF-κB(p65)	Forward 5′-GCGACCATTGTTAGCCACATACG-3′
	Reverse5′-CGTTGATGTCGCACAGAGGGAT-3′

Plasmids and shRNA

plk0.1 *MEN1* shRNA and pcDNA3.1 MEN1 were kindly provided by Dr. Guanghui Jin (Canaff et al., 2012). GFP-MEN1 and GFP-MEN1(277-541) were generated by inserting target genes or gene fragments amplified by PCR into the pEGFP-C3 vector (Clonetech). GFP-NES-MEN1 was generated by inserting MEN1 into a GFP-NES vector. GFP-MEN1 (D418D), GFP-MEN1 (A541T), and GFP-MEN1 (G503D) mutations were generated by site-directed mutagenesis (Stratagene); Primer sequences used for plasmids construction are listed below:

MEN1 (pEGFP-C3)	Forward5′-GGAATTCTGATGGGGCTGAAGGCCGCCCAG-3′
	Reverse5′-CGGGATCCTCAGAGGCCTTTGCGCTGC-3′
MEN1(D418D) (pEGFP-C3)	Forward5′-CTGCGATTCTACGATGGCATCTGCAAATGGGAGGAGGG-3′
	Reverse5′-TTGCAGATGCCATCGTAGAATCGCAGCAGGTGGGCG-3′
MEN1(G503D) (pEGFP-C3)	Forward5′-TTGCAGATGCCATCGTAGAATCGCAGCAGGTGGGCG-3′
	Reverse5′-GGTGGTGATGCCGCGGGTGCTGGCACCTGAGCC-3′
MEN1(A541T) (pEGFP-C3)	Forward5′-CACTGGACAAGGACCTGGGCACCGGCCAGGGT-3′
	Reverse5′-CGGTGCCCAGGTCCTTGTCCAGTGCTGGCTTCT-3′
NES-MEN1(pEGFP-C3)	Forward5′- CCCAAGCTTATGGGGCTGAAGGCCGCC-3′
	Reverse5′- CGGGATCCTCAGAGGCCTTTGCGCTGCC-3′
MEN1-277∼541(pEGFP-C3)	Forward5′-ACATCTGGAAAGGTACGCATCACCACCGCCGGA-3′
	Reverse5′-CGGTGGTGATGCGTACCTTTCCAGATGTCCCAGGTC-3′

The *shMEN1* vector was constructed by inserting *shRNA* hairpin sequences into a mU6pro vector. The *shMEN1* sequence is as follows: 5′-TGCTCCGACTCTTATCTGTGTTCAAGAGACACAGATAAGAGTCGGAGCTTTTTTC-3′;3′-TCGAGAAAAAAGCTCCGACTCTTATCTGTGTCTCTTGAACACAGATAAGAGTCGGAGCA-5′.

NF-κB promoter-luciferase reporter assay

The NF-κB promoter-luciferase vector was generated by inserting a 100-bp fragment comprising the mouse NF-κB promoter region into a pGM-lu vector. Astrocytes or HEK293T cells were transfected with the NF-κB promoter-luciferase vector together with dual reporter plasmid pRL-TK using Lipofectamine LTX and Plus Reagent (Invitrogen). Cell lysates were generated using a passive lysis buffer (PLB) (Promega). Firefly and Renilla luciferase activity was measured in cell lysates according to the manufacturer's instructions using a Dual Luciferase Assay System with a Turner TD-20/20 luminometer (Turner Designs, Sunnyvale, CA, USA). Relative firefly luciferase activity was calculated by normalizing transfection efficiency to Renilla luciferase activity. The mouse NF-κB promoter region comprised the following sequence: GGCCTAACTGGCCGGTACCGCTAGCCTCGATGGGAATTTCCGGGAATTTCCGGGAATTTCCGGAATTTCCGCGCGTAGATCTGCAGAAGCTTAGACACT

Golgi staining

Golgi staining was performed using the FD Rapid Golgi Stain kit according to the manufacturer's instructions (FD Neuro Technologies). Freshly dissected brains were immersed in the impregnation solution, comprising equal volumes of Solutions A and B, and stored at room temperature for 2 weeks in the dark. Then brains were transferred into Solution C and stored at 4°C in the dark for at least 48 hours. Brains were then sectioned using a vibratome (Leica 1200S) at a thickness of 200 μm. Brain sections were then stained with Solutions D and E. Golgi-stained neurons and dendritic segments from cortex and hippocampus were imaged by microscopy. Dendritic branching and spines were analyzed using NIH ImageJ software.

Co-immunoprecipitation

Brain or cell lysates were pre-cleared with protein A-Sepharose beads. Menin or GFP proteins were precipitated by adding anti-menin or GFP antibodies. After incubation for 2 hours at 4°C, complexes were precipitated with 10 μL of protein A-Sepharose beads with gentle agitation at 4°C for 4 hours; nonspecific IgG was used as a negative control. Beads were washed, and the immunoprecipitated protein complex was loaded onto a 12% SDS-PAGE gel and processed for western blotting.

Enzyme Linked Immunosorbent Assay (ELISA)

IL-1β, Cortisol and Serotonin (5-HT) levels in cell culture supernatant, serum or tissues were measured using mouse IL-1β, Cortisol and 5-HT ELISA Kits (R&D-Valukine Elisa Kit, Cat: VAL601; R&D-Parameter Elisa Kit, Cat: KGE008B; Shanghai Meilian, mouse 5-HT Elisa kit, Cat: M1001891) according to the manufacturer's instructions.

Electrophoretic Mobility Shift Assay (EMSA)

EMSA reactions comprised 1ng of a 5′-labeled DNA probe, 12.5 ng/μl of an equimolar mix of Poly (dI-dC) and Poly (dA-dT) non-specific DNA competitor and lysates from cells transfected with various vector constructs. Reactions were incubated at 37°C for 20 min and separated on 6% acrylamide–bisacrylamide non-denaturing gels using 0.5 × Tris–borate–EDTA buffer, pH 8.3 (TBE). Samples were subjected to electrophoresis for 2 hours at 100V using ice-cold 0.5 × TBE buffer, and DNA was transferred onto Hybond-N+ membranes (GE Healthcare) by blotting at 250 mA for 60 min using a semidry transfer unit, followed by UV cross-linking. The biotin-labeled DNA was visualized using a Phototope-Star detection kit (Thermo, USA).

Immunofluorescence

Mouse brain sections or cultured cells were washed three times with PBS and antigen retrieval was performed using citrate buffer (pH 7.0); samples were then permeabilized and blocked in PBS containing 0.5% Triton X-100 and 10% normal goat serum at room temperature for 1 h. Sections were incubated with primary antibodies in blocking buffer overnight at 4°C. After washing, secondary antibodies were added to the blocking buffer and incubated for one hour. Samples were then washed, and counterstained with DAPI. Images were acquired using a Nikon confocal microscope.

Primary antibodies used for immunostaining include: menin (rabbit, 1:1000; Abcam, Ab4452), p65 (rabbit, 1:1000; Cell Signaling Technology, #8242), GFAP (mouse, 1:500; Cell Signaling Technology, #3670), NeuN (mouse, 1:1000; Millipore, #MAB377), Iba1 (Mouse, 1:300; Santa cruz, Sc-32725), CC1 (mouse, 1:500; Millipore, #OP80), PDGFRα (mouse, 1:500; R&D, #AF1062), MBP (rabbit, 1:500; Santa Cruz, #Sc13914), GFAP (goat, 1:500; Santa Cruz, #Sc6170). 488/594 donkey anti-mouse/rabbit secondary antibodies (1:1000) and Mounting Medium with DAPI was purchased from Invitrogen.

Protein stability assays

GFP-tagged MEN1 or MEN1 mutation constructs were transfected into HEK293T cells treated with cycloheximide (CHX) at 200 μg/mL at different time points. Proteins were extracted and subjected to western blotting; GFP-tagged menin proteins were detected using an anti-GFP antibody. Turnover of WT-menin/menin variants was quantified using ImageJ.

Electrophysiology

For hippocampal slice recordings, 400 μm horizontal slices from control and GcKO mice were prepared using a Leica LS1200s vibrating microtome in ice cold oxygenated artificial cerebrospinal fluid (aCSF) (120 mM NaCl, 3.5 mM KCl, 1.25 Mm NaH_2PO_4, 26 mM $NaHCO_3$, 10 mM D-glucose, 1.3 mM $MgSO_4$, 2.5 mM $CaCl_2$, PH = 7.4, 290-320 mOsm). Slices were transferred to a chamber and held at 32°C for 1 hour and at room temperature for an additional hour. All recordings were performed at room temperature. Mice were divided into three groups (Ctrl, GcKO with vehicle control, and GcKO with IL-1β-RA groups). IL-1β–RA was used at a concentration of 200 μg/μl.

Schaffer collateral inputs to the CA1 region were stimulated with a bipolar tungsten electrode. Field excitatory postsynaptic potentials (fEPSPs) were recorded from neurons within the CA1 dendritic layer by insertion of an electrode in the Schaffer collateral pathway as the stimulating electrode. Based on the stimulus–response curve, a stimulation intensity that evoked a fEPSP within 30% of the maximum response was selected and recorded for 20 min to establish a baseline. LTP was then induced with a two-train high-frequency stimulus (100 Hz-30 s interval). The field potential response following tetanic stimulation was recorded for 60 min. The LTP magnitude was quantified as the percentage change in the average fEPSP slope over 60 min after LTP induction.

MEN1 coding regions sequencing

Genomic DNA used for analysis was extracted from peripheral white blood cells using standard phenol-chloroform extraction methods. Coding exons of the *MEN1* gene were confirmed using NCBI and Ensemble websites. *MEN1* coding exons were amplified by PCR, and the PCR products were bi-directionally characterized by Sanger sequencing (Sino Geno Max Company, Beijing, China). Primers were designed using NCBI BLAST, and synthesized by Idobio Biological Technology (Beijing, China).

Behavioral Studies

Forced Swimming Test

The forced swim test (FST) was used to assess depressive-like behavior. Mice were placed in a container filled with water that eventually resulted in immobility, reflecting behavioral despair. Water (23 ± 1°C) was placed in a transparent acrylic cylinder bath (10cm in diameter, 20cm in height) filled to a depth of 13cm. Mice were placed in the water for six minutes using a video tracking system (Smart 3.0); immobility duration (%) within the final 5 min of testing was recorded.

Tail Suspension Test

Mice were suspended by their tails from an acrylic bar (15cm in diameter, 30cm in height) for six minutes and monitored using a video tracking system (Smart 3.0). Escape-related behavior was assessed, where immobility duration (%) during the 6 min suspension period was recorded.

Social Interaction

The test apparatus for social interaction comprised three rectangular chambers (18 × 35 × 18 cm) divided by plexiglass walls with openings (6 × 5 cm) which allowed animals to move between chambers. Both side chambers contained an empty transparent plexiglass holder (8 cm in diameter, 10 cm high), with small holes allowing snout contact. The width of the holes were of a sufficiently small size to prevent biting or aggressive interactions between the animals. A test mouse was first released into the central chamber and was allowed to habituate for 5 min. An unfamiliar gender- and age-matched stranger mouse was then placed in one of the holders. The location of the stranger mouse in either of the two holders (the social chamber) varied systematically between trials. The test mouse was allowed to explore the apparatus for 10 min. At the end of the 10 min duration, a novel mouse was placed in the other holder. The test mouse was allowed to explore the entire apparatus for 10 min. Time spent in sniffing each holder was recorded using a video camera.

Sucrose Preference Test (SPT) and Sucrose Consumption Test (SCT)

Animals were first trained to consume a 1% sucrose solution from two differing bottles (48 hours before the formal experiment). Twenty-four hours later, the animals were allowed free access to 1% sucrose and water from two differing bottles. To avoid bottle side preference, the two bottles were switched. The amounts in the two bottles were measured after 24 hours and sucrose preference was calculated according to the following formula: Sucrose preferences (%) = sucrose consumption / (sucrose + water consumption) × 100%.

Rotarod Test

Mice were placed on a stationary rotarod (AccuRotor Rota Rod Tall Unit, 63-cm fall height, 30-mm diameter rotating dowel; Accuscan, Columbus, OH). The dowel was then accelerated to 60 rpm/min, and the latency to fall (in seconds) was recorded. The procedure was repeated over 4 consecutive trials, which was averaged to yield the daily latency to fall for each mouse. If an animal fell off the rotarod rapidly (e.g., due to inattention or slips), they were placed back on the rotarod for an additional trial, and the latency was not included in the daily average. The entire procedure was repeated for 2 additional days for a total of 3 days. In addition to the average latency across the 4 trials per day, the maximum latency to fall per day was also analyzed.

Open Field Test

To explore locomotion and spontaneous activity, we characterized mouse behavior as they freely explored an open-field plastic chamber (40-cm width × 40-cm length × 30-cm height) using a video tracking system (Smart 3.0). Two month old mice were placed in this arena for 10 min., and total distance and time spent in the center region (20cm × 20cm) was recorded.

Elevated Plus Maze

The apparatus comprised two opposing open arms (50 × 10 cm) and two opposing closed arms with roofless gray walls (40 cm) connected by a central square platform and positioned 50 cm above the ground. Mice were placed in the open arms facing an open arm, and their behavior was tracked for 5 min with an overhead camera and Smart 3.0 software. Time spent in the open arms (%) was reported.

Morris Water Maze

The water maze used in this study comprised a circular tank 120 cm in diameter with a platform filled with tap water at a temperature of 22 ± 2°C. Different shapes were posted along the walls of the tank, which served as spatial reference cues. A camera was mounted above the maze to record the swimming traces in the water maze. During the acquisition trials, the platform was submerged 1-2 cm below the water surface, mice were place into the maze at one of four points (N, S, E, W) facing the wall of the tank. Mice were allowed to search for a platform for 60 s. If a mouse failed to find the platform, it was guided to the platform and maintained on the platform for 10 s. Four trials a day were conducted with an intermission of 1h minimum between trials. Escape latency indicative of spatial memory acquisition, was recorded for each trial. On day 7, the platform was removed and a probe test was conducted. The percentage time spent in each of the four quadrants and the number of target (platform) area crossings, mean speed, total distance was recorded.

RNA-Sequencing analysis

Primary astrocytes from control or GcKO mice were cultured as described in the main text. Isolated RNA was subsequently used for RNA-seq analysis. cDNA library construction and sequencing was performed by the Beijing Genomics Institute using BGISEQ-500 platform. High-quality reads were aligned to the mouse reference genome using Bowtie2. Expression levels for each of the genes were normalized to fragments per kilobase of exon model per million mapped reads (FPKM) using RNA-seq by Expectation Maximization (RSEM). We identified DEGs (differential expressed genes) between samples and performed clustering analysis and functional annotation. Genes with $\geq$ 2-fold change and false discovery rates (FDR) of $\leq$ 0.001 were considered to be statistically significant. Pathways overrepresented by DEGs were annotated in the KEGG (Kyoto Encyclopedia of Genes and Genomes) database.

QUANTIFICATION AND STATISTICAL ANALYSIS

Statistical analysis

All data presented are expressed as arithmetic mean ± SEM. All statistical analyses were performed using GraphPad Prism version 5.0. Null hypotheses were rejected at p values equal to or higher than 0.05. For statistical comparisons between two groups, we first performed a Shapiro-Wilk normality test (Prism) to determine whether the data was likely normally distributed. For normally-distributed data, we used unpaired Student's t tests to evaluate statistical significance of differences between the two groups. Statistically significant differences between groups were determined using one-way ANOVA. In evaluating multiple comparisons, Tukey's correction method was used to adjust p values accordingly to lower the probability of type I errors.

All electrophysiological results were analyzed using Sigma Stat 4 statistical software. Statistical significance was evaluated by one-way ANOVA with Holm-Sidak pairwise tests. Values of $p < 0.05$ were considered to be statistically significant. DNASTAR Laser gene software (version 7.1) was used to analyze Sanger sequencing data. Hardy–Weinberg equilibrium (HWE) for genotypic distributions of all detected SNPs were examined using chi-square (X^2) goodness-of-fit tests. The chi-square test was applied to analyze differences in genotypic distribution between MDD patients and controls.

Description of sample size (n-number)

For behavior tests described in the study, the number of mice analyzed in each group are described in the respective Figure Legends (Figures 1A, 1B, 2, and 4); the number of slices and mice used for electrophysiological recordings is defined. For other experiments (Western Blotting, Immunofluorescence, Golgi stains, CO-IP, Luciferase assay and Electrophysiology), the definition of "n" in the context of independent experimental repeats are described in respective Figure Legends. All statistical details, including the exact value of n, what n represents, and which statistical test was performed, is described in the Figure Legends.

DATA AND SOFTWARE AVAILABILITY

The SRA accession number for RNA-seq data reported in this paper is SRA: SRP151969.

Neuron, Volume *100*

Supplemental Information

Menin Deficiency Leads to Depressive-like Behaviors in Mice by Modulating Astrocyte-Mediated Neuroinflammation

Lige Leng, Kai Zhuang, Zeyue Liu, Changquan Huang, Yuehong Gao, Guimiao Chen, Hui Lin, Yu Hu, Di Wu, Meng Shi, Wenting Xie, Hao Sun, Zhicheng Shao, Huifang Li, Kunkun Zhang, Wei Mo, Timothy Y. Huang, Maoqiang Xue, Zengqiang Yuan, Xia Zhang, Guojun Bu, Huaxi Xu, Qi Xu, and Jie Zhang

Supplemental Information for

Menin deficiency leads to depressive-like behaviors in mice by modulating astrocyte-mediated neuroinflammation

Inventory of Supplemental Information:

Supplemental Figures and Figure Legends:

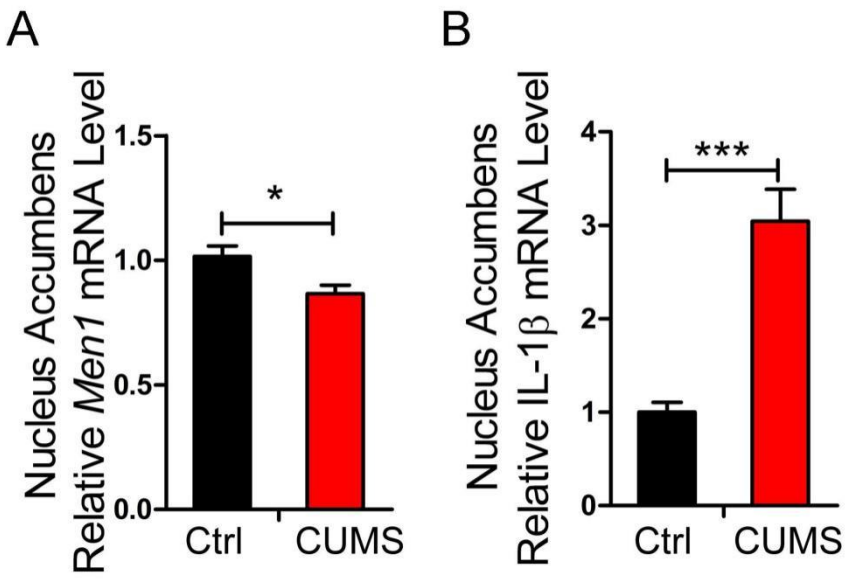

Figure S1. Mouse menin levels are attenuated and IL-1β levels are elevated in the Nucleus accumbens after CUMS, related to Figure 1 and Figure 3.

Male C57BL/6 mice were exposed to chronic unpredictable mild stress (CUMS).

A. *Men1* mRNA levels in the Nucleus accumbens of CUMS/Control mouse brain. n=6 experimental replicates/group.

B. *IL-1β* mRNA levels in the Nucleus accumbens of CUMS/Control mouse brain. n=6 experimental replicates/group.

Data represent mean±SEM, *p<0.05, ***p<0.001, one-way ANOVA with Turkey post hoc test.

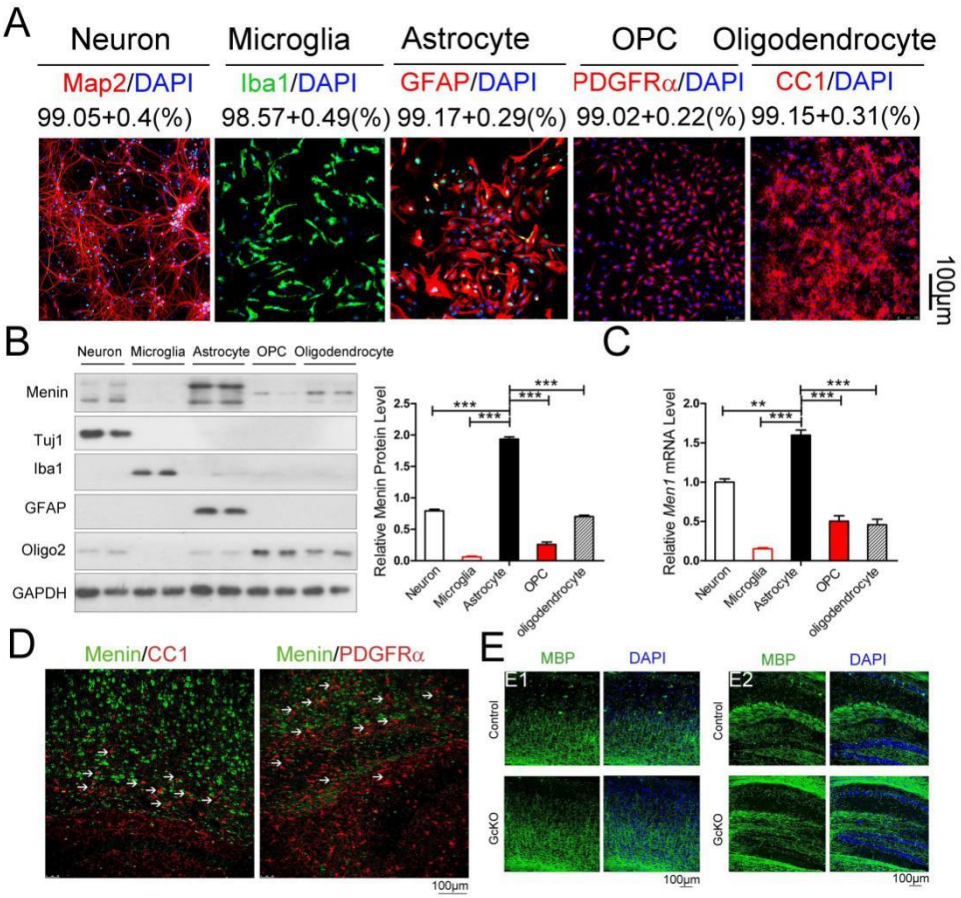

Figure S2. Menin expression in neurons, microglia, astrocytes, and oligodendrocyte progenitor cells (OPCs), and oligodendrocytes in GcKO and control mouse brain, related to Figure 1 and 2.

(A) Primary neurons, astrocytes, microglia, OPCs and oligodendrocytes were cultured as described in Methods. Neurons were stained with MAP2 and DAPI; astrocytes were stained with GFAP and DAPI, Microglia were stained with Iba1 and DAPI; OPC were stained with PDGFRα and DAPI; Oligodendrocytes were stained with CC1 (Anti-adenomatous polyposis coli-APC) and DAPI; as indicated in Red (Iba1: Green) and Blue respectively. Scale bar: 100um. Purity of primary neurons or astrocyte cultures were also provided respectively.

(B-C) Menin levels were detected by western blotting (B) and Real-time PCR (C) in the indicated cell types (neurons, microglia, astrocyte, OPC and Oligodendrocyte). TuJ1, Iba1, GFAP and Oligo2 were used as cell-specific markers for neurons, microglia, astrocytes and oligodendrocytes respectively, GAPDH served as a loading control. Data represent mean±SEM, n=3 experimental replicates/group; **p<0.01, ***p<0.001, one-way ANOVA with Tukey's post hoc test.

(D) Double immunofluorescence staining of menin (green) with CC1 (Red) or PDGFRα (red) in mouse cortex regions. Arrows indicate that menin is barely detectable in oligodendrocytes *in vivo* (Scale bar: 100μm)

(E) MBP (Myelin basic protein) staining in cortex (E1) and hippocampus (E2) of GcKO/control mice indicates that myelination is not significantly changed in GcKO animals. (Scale bar: 100μm)

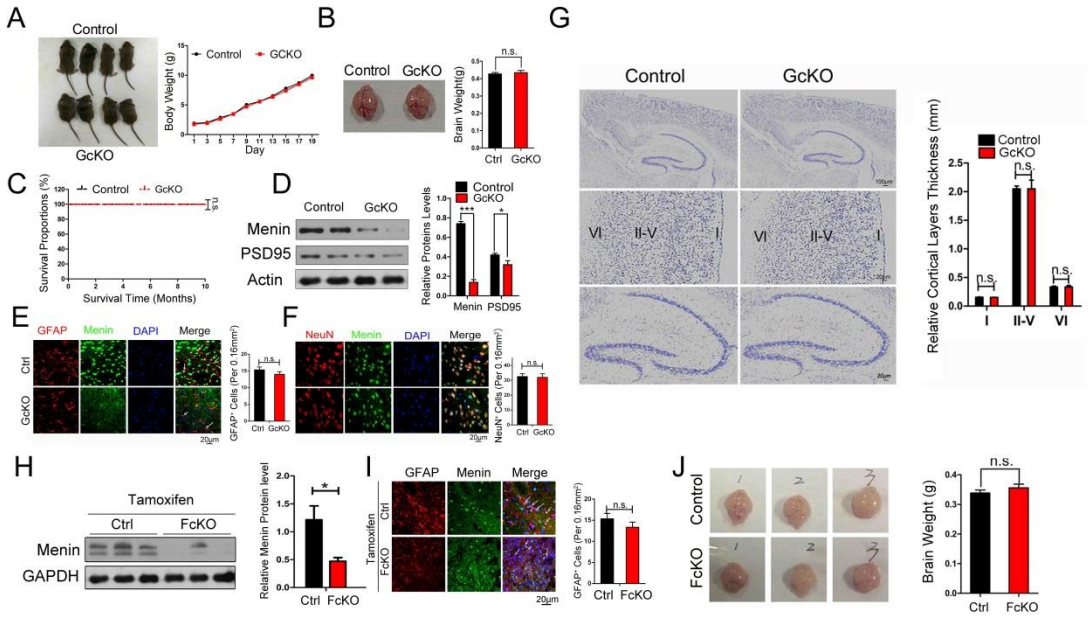

Figure S3. *GFAP-Cre* and *Fgfr3-iCre(ER)* mediated *Men1* reduction in mice (GcKO and FcKO), related to Figure 2.

(A) Body weight of GcKO and littermate Control mice (control：n=20 mice；GcKO: n=12 mice).

(B) Brain weight of one-month old GcKO and littermate control mice.

(C) Kaplan-Meier survival curves from GcKO and control mice. (Control mice: n>50, GcKO mice: n>50).

(D) Menin and PSD95 protein levels were significantly lower in cortex from GcKO mice compared to controls. n = 3 mice per group.

(E-F) Double immunofluorescence staining of menin (green) with GFAP (E) or NeuN (F) reveal reductions in menin expression in astrocytes in GcKO mouse cortex. (Scale bar: 20μm). Astrocyte and neuron numbers were also quantified and presented in the adjacent panels (right). n > 100 cells from 6 slices from 3 mice respectively.

(G) Brain sections from postnatal three-month GcKO and Control mice were subjected to Nissl staining. Layer I, Layer II-V, and Layer VI measurements were quantified by Image J. Scale bar: 100μm, 20μm, 20μm respectively.

(H-J) Tamoxifen-induced menin reduction in FcKO mice; (H) Menin protein levels were significantly reduced in tamoxifen-treated FcKO mouse cortex compared to controls. n=3 mice per group. (I) Double immunofluorescence staining to detect menin (green) and GFAP (red) in tamoxifen-treated FcKO and control mouse cortex; menin expression is markedly reduced in astrocytes in FcKO mouse cortex (Scale bar: 20μm). Astrocyte numbers was also quantified and presented in the panels on the righthand side. n > 100 cells from 6 slices from3 mice respectively.

(J) No significant difference in brain weight was observed between 1 month old FcKO and control mice. (Control： n=11 mice；FcKO: n=10 mice)

Data represent mean±SEM, n.s.: not significant, *p<0.05, ***p<0.001, A, unpaired t test，B-J, one-way ANOVA with Tukey's post hoc analysis.

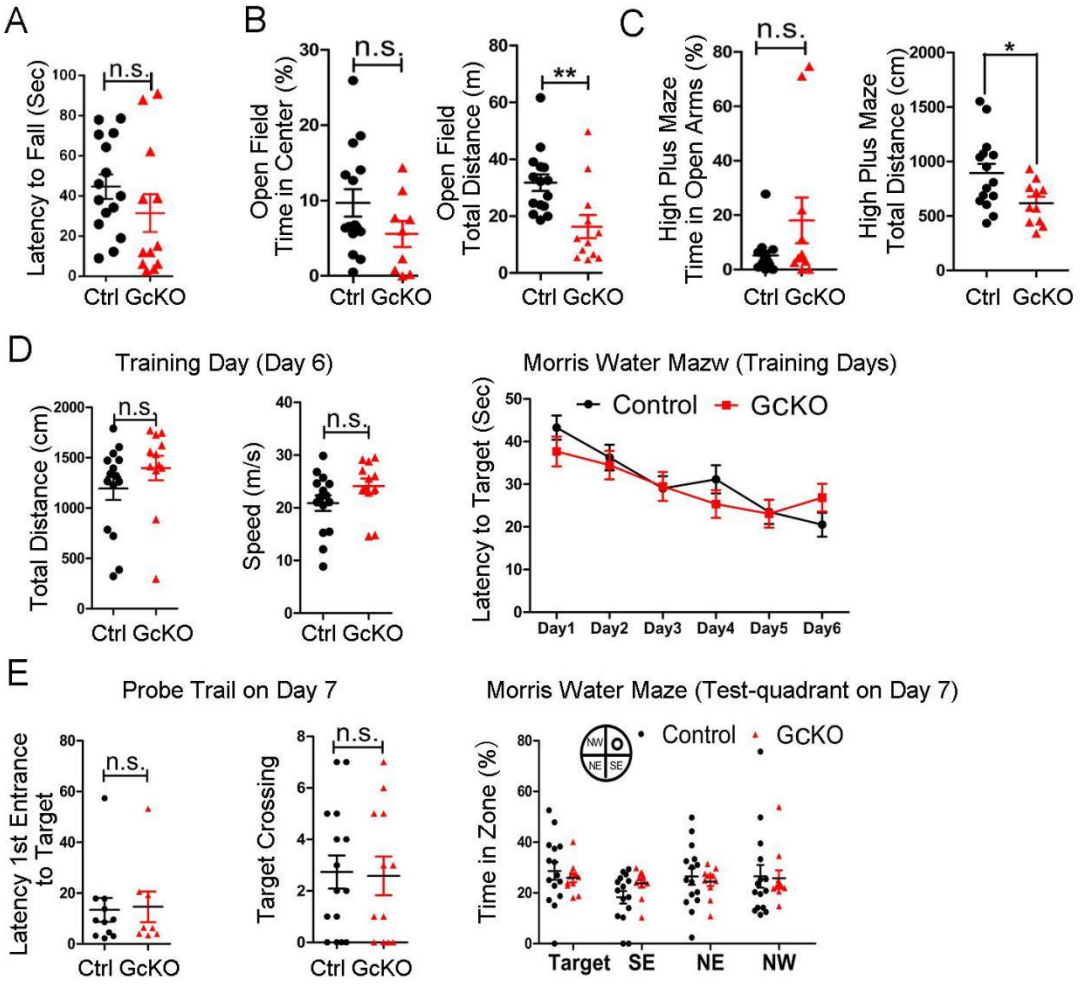

Figure S4. Behavioral tests in GcKO and control mice, related to Figure 2.

(A) GcKO and control mice behavior in Rotarod tests.

(B) GcKO and control mice behavior in Open field tests.

(C) GcKO and control mice behavior in High plus maze tests.

(D-E) GcKO and control mice behavior in Morris Water Maze test.

(Control: n=15mice； GcKO: n=12 mice) Data represent mean±SEM, n.s.: not significant,*p<0.05, **p<0.01, one-way ANOVA with Tukey's post hoc analysis.

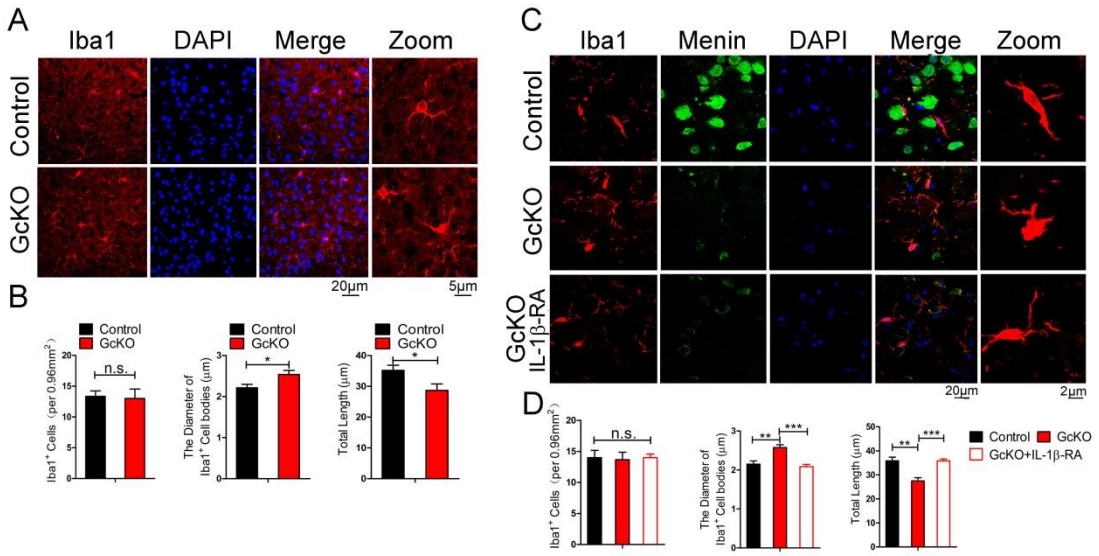

Figure S5. Iba1 staining in the mPFC region of control and GcKO mice treated with IL-1β-RA, related to Figure 3 and Figure 5.

(A) GcKO and control mice brain slices were subjected to Iba1 (red) and DAPI (blue) staining. Scale bar: 20μm, 5μm respectively.

(B) Characterizing Iba1-positive cells number, morphological parameters include cell body size and total processes length in microglia. At least 20 cells each from three mice were selected to quantify the morphological parameters. (n > 20 cells from 6 slices from 3 mice respectively)

(C) Iba1 staining in the mPFC region of Control and GcKO mice treated with saline or IL-1β-RA. Scale bar: 20μm, 5μm respectively.

(D) Analyses of Iba1 positive cell number, size of cell body and total processes length in microglia. At least 20 cells each from three mice were selected to quantify the morphological parameters. (n > 20 cells from 6 slices from 3 mice respectively)

Data represent mean±SEM. n.s.: not significant, *p<0.05, **p<0.01, ***p<0.001, one-way ANOVA with Tukey's post hoc analysis.

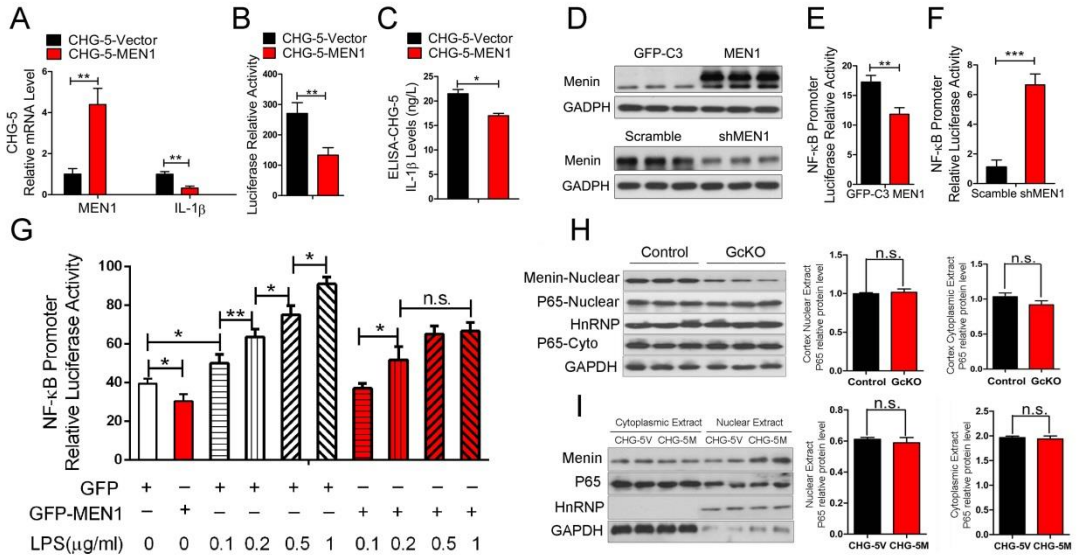

Figure S6. p65 subcellular localization, IL-1β expression and NFκB-mediated transactivation in CHG5 and HEK293 cells with LPS, related to Figure 3.

(A) MEN1 and IL-1β expression levels as determined by qRT-PCR in CHG5-MEN1 stable and control cells. Menin protein expression is shown in the lower panel. n=3 experimental replicates/group.

(B) NFκB-mediated transactivation in CHG5 cells with stable MEN1 overexpression compared to controls. n = 6/group/experiment.

(C) IL-1β protein levels in CHG5 cells measured by ELISA. n=6 experimental replicates/group.

(D) Menin expression in HEK293T cells transfected with GFP control, GFP-MEN1, scrambled siRNA, or shMEN1 siRNA.

(E-F) NFκB-mediated transactivation in HEK293T cells with menin overexpression (E) or knockdown (F). n=6 experimental replicates/group.

(G) HEK293T cells were transfected with GFP and GFP-MEN1 plasmids, and subsequently treated with LPS as indicated. NFκB-dependent transactivation was measured by Luciferase assay.

(H) Menin and p65 protein levels in cytoplasmic and nuclear fractions from GcKO and control mouse brain cortex. Quantification of p65 levels are shown in the right panels, n=3 experimental replicates/group.

(I) Menin and p65 protein levels in cytoplasmic and nuclear fractions from CHG-5 control vector (CHG-5V) and CHG-5-MEN1 (CHG-5M) stably expressing cell lines. Quantification of p65 levels are shown in the right panels, n=3 experimental replicates/group.

Data represent mean±SEM, n.s.: not significant, *p<0.05, **p<0.01, ***p<0.001, one-way ANOVA with Tukey's post hoc analysis.

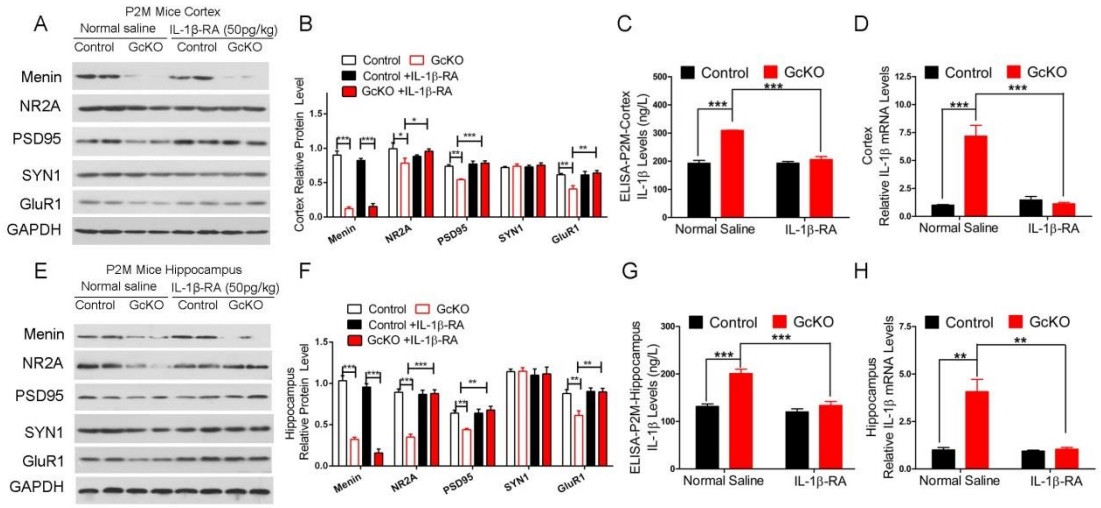

Figure S7. Synaptic proteins levels and IL-1β expression in GcKO and control mice treated with saline or IL-1β-RA, related to Figure 5.

Two-month old GcKO and littermate controls mice treated with an NF-κB inhibitor (PDTC) or an IL-1β-R-Antagonist (IL-1β-RA) for 7 days. After behavioral analysis, cortex and hippocampus were processed for western blotting, ELISA and RT-PCR. Western blot analysis of protein expression in cortex (A-B) and hippocampus of GcKO (E-F) and control mice received saline or IL-1β-RA. Immunoblots were probed with antibodies against the indicated proteins. n=4 experimental replicates/group. IL-1β protein and mRNA levels were measured in cortex (C-D) and hippocampus (G-H) of GcKO and control mice treated with saline or IL-1β-RA. n=4 experimental replicates/group.

Data represent mean±SEM. *p<0.05, **p<0.01, ***p<0.001, one-way ANOVA with Tukey's post hoc analysis.

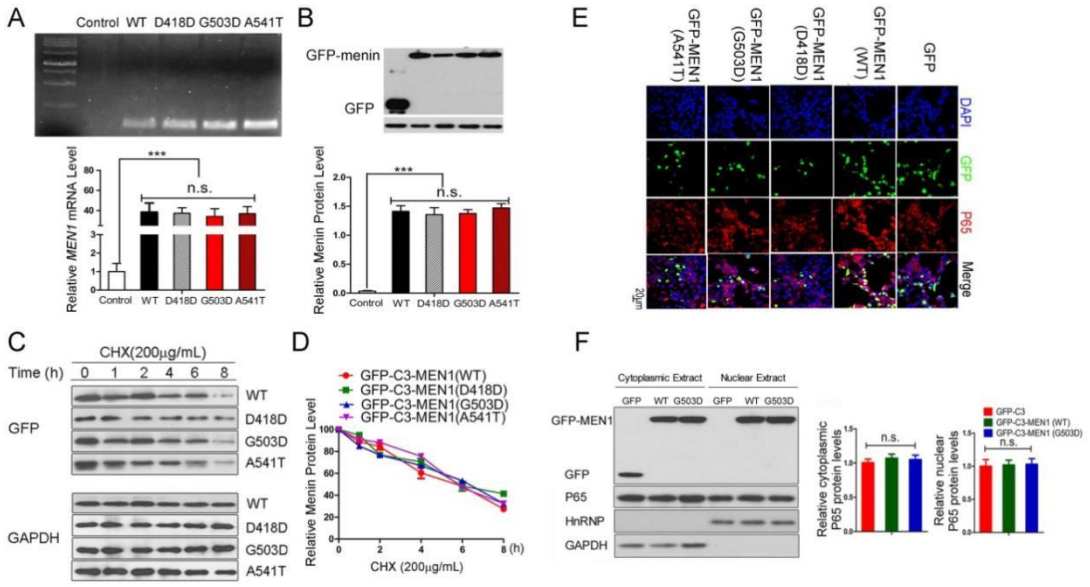

Figure S8. rs375804228 (G503D) does not alter transcription, protein expression, protein turnover, or cellular localization profiles in menin, related to Figure 6.

(A-B) HEK293T cells transfected with a GFP control vector, or GFP-WT-MEN1, GFP-MEN1-G503D, GFP-MEN1-D418D, and GFP-MEN1-A541T were processed for mRNA (A) and protein (B) expression analysis by qRT-PCR/Western blotting. Quantitation is shown in the bottom panels. n = 6 experimental replicates/group.

(C-D) HEK293T cells were transfected with GFP control vector, GFP-WT-MEN1, GFP-MEN1(G503D), GFP-MEN1(D418D), and GFP-MEN1(A541T) constructs. Cells were exposed to cycloheximide for the time indicated, and menin degradation was determined by western blotting. Representative blots are shown in panel C; Quantification of menin protein turnover is shown in D. Menin levels were standardized to GAPDH and normalized to time 0 (set to 100%). n=3 experimental replicates/group.

(E) Menin and p65 localization was determined by GFP and p65 co-staining in HEK293T cells transfected with GFP, GFP-MEN1(WT), GFP-MEN1(D418D), GFP-MEN1(G503D) and GFP-MEN1(A541T) plasmids. (Scale bar: 20μm).

(F) p65 protein levels in HEK293T cytoplasmic and nuclear fractions in cells transfected with GFP, GFP-MEN1 or GFP-MEN1(G503D) as determined by western blotting. Quantification of band intensities are presented on right panel, n=3 experimental replicates/group.

Data represent mean ± SEM. n.s.: not significant, ***$p<0.01$, one-way ANOVA with Turkey post hoc test.